One year of Galileo dust data from the Jovian system: 1996

H. Krüger[a,*], E. Grün[a], A. Graps[a], D. Bindschadler[b], S. Dermott[c], H. Fechtig[a], B.A. Gustafson[c], D.P. Hamilton[d], M.S. Hanner[b], M. Horányi[e], J. Kissel[f], B.A. Lindblad[g], D. Linkert[a], G. Linkert[a], I. Mann[h,i], J.A.M. McDonnell[j], G.E. Morfill[f], C. Polanskey[b,,], G. Schwehm[i], R. Srama[a], H.A. Zook[k,1]

[a] *Max-Planck-Institut für Kernphysik, Postfach 10 39 80, 69029 Heidelberg, Germany*
[b] *Jet Propulsion Laboratory, Pasadena, California 91109, USA*
[c] *University of Florida, Gainesville, FL 32611, USA*
[d] *University of Maryland, College Park, MD 20742-2421, USA*
[e] *Laboratory for Atmospheric and Space Physics, Univ. of Colorado, Boulder, CO 80309, USA*
[f] *Max-Planck-Institut für Extraterrestrische Physik, 85748 Garching, Germany*
[g] *Lund Observatory, 221 Lund, Sweden*
[h] *Institut für Planetologie, Universität Münster, 48149 Münster, Germany*
[i] *ESTEC, 2200 AG Noordwijk, The Netherlands*
[j] *Planetary and Space Science Research Institute, The Open University, Milton Keynes, MK7 6AA, UK*
[k] *NASA Johnson Space Center, Houston, Texas 77058, USA*

Received 5 January 2001; accepted 15 May 2001

Abstract

The dust detector system onboard Galileo has recoding dust impacts in circumjovian space since the spacecraft was injected into a bound orbit about Jupiter in December 1995. This is the sixth in a series of papers dedicated to presenting Galileo and Ulysses dust data. We present data from the Galileo dust instrument for the period January to December 1996 when the spacecraft completed four orbits about Jupiter (G1, G2, C3 and E4). Data were obtained as high-resolution realtime science data or recorded data during a time period of 100 days, or via memory read-outs during the remaining times. Because the data transmission rate of the spacecraft is very low, the complete data set (i.e. all parameters measured by the instrument during impact of a dust particle) for only 2% (5353) of all particles detected could be transmitted to Earth; the other particles were only counted. Together with the data for 2883 particles detected during Galileo's interplanetary cruise and published earlier, complete data of 8236 particles detected by the Galileo dust instrument from 1989 to 1996 are now available. The majority of particles detected are tiny grains (about 10 nm in radius) originating from Jupiter's innermost Galilean moon Io. These grains have been detected throughout the Jovian system and the highest impact rates exceeded 100 min^{-1}. A small number of grains has been detected in the close vicinity of the Galilean moons Europa, Ganymede and Callisto which belong to impact-generated dust clouds formed by (mostly submicrometer sized) ejecta from the surfaces of the moons (Krüger et al., 1999e. Nature 399, 558). Impacts of submicrometer to micrometer sized grains have been detected throughout the Jovian system and especially in the region between the Galilean moons. © 2001 Elsevier Science Ltd. All rights reserved.

1. Introduction

In December 1995, Galileo became the first artificial satellite to orbit Jupiter. The main goals of the Galileo mission are the exploration of the giant planet itself, its four Galilean satellites and its huge magnetosphere. Galileo carries a highly sensitive impact ionization dust detector on board, which is a twin of the dust detector on the Ulysses spacecraft (Grün et al., 1992a,b; 1995c). Dust data from both spacecraft have been used many times for the analysis of, e.g. the interplanetary dust complex, dust related to asteroids and comets, interstellar dust grains sweeping through the solar system, and streams of dust particles originating from the Jupiter system. Here we recall only publications which are related to dust in the Jupiter system. See Krüger et al. (1999b, d) for a summary of references to other works.

Streams of dust particles originating from the Jovian system have been discovered with the Ulysses detector (Grün et al., 1993) and later been confirmed by Galileo (Baguhl et al., 1995; Grün et al., 1996a). The first dust detection with Galileo in the Jupiter system itself was reported from Galileo's initial approach to Jupiter and Io fly-by in December 1995 (Grün et al., 1996b). At least three different types of dust particles have been identified in the Jupiter system (Grün et al., 1997; 1998): (1) Streams of dust particles with high and variable impact rates throughout Jupiter's magnetosphere. The particles are about 10 nm in diameter (Zook et al., 1996; Liou, 1997) and they originate from the innermost Galilean satellite Io (Krüger et al., 1999a; Graps et al., 2000). Because of their small sizes the particles strongly interact with Jupiter's magnetosphere (Horányi et al., 1997; Heck, 1998). These streams of particles have been used to analyse the field of view of the dust detector (Krüger et al., 1999d) at a level of detail which could not be achieved during ground calibration. (2) Sub-micrometer grains which form dust clouds surrounding the Galilean moons (Krüger et al., 1999e, 2000). These grains are ejected from the satellites' surfaces by hypervelocity impacts of interplanetary dust particles. (3) Bigger micrometer-sized grains forming a tenuous dust ring between the Galilean satellites. This third group is composed of two subpopulations, one orbiting Jupiter on prograde orbits and a second one on retrograde orbits (Colwell et al., 1998; Thiessenhusen et al., 2000). Most of the prograde population is maintained by grains escaping from the clouds surrounding the Galilean satellites (Krivov et al., 2001).

This is the sixth paper in a series dedicated to presenting both raw and reduced data from the Galileo and Ulysses dust instruments. The reduction process of Galileo and Ulysses dust data has been described by Grün et al. (1995c) (hereafter Paper I). In Papers II and IV (Grün et al., 1995a; Krüger et al., 1999b) we present the Galileo data set spanning the 6-year time period October 1989 to December 1995. Papers III and V (Grün et al., 1995b; Krüger et al., 1999d) discuss the five years of Ulysses data from October 1990 to December 1995. The present paper extends the Galileo data set from January to December 1996, which is part of Galileo's prime Jupiter mission. A companion paper (Krüger et al., 2001) (Paper VII) details Ulysses' measurements from 1996 to 1999.

The main data products are a table of the number of all impacts determined from the accumulators of the dust instrument and a table of both raw and reduced data of all "big" impacts received on the ground (the term "big" applies to impacts in ion amplitude ranges AR2 to AR6; see Section 3 in this paper and Paper I for a definition of the amplitude ranges). The information presented in this paper is similar to data which we are submitting to the various data archiving centers (Planetary Data System, NSSDC). The only difference is that the paper version does not contain the full data set of the large number of "small" particles (amplitude range AR1), and the numbers of impacts de-
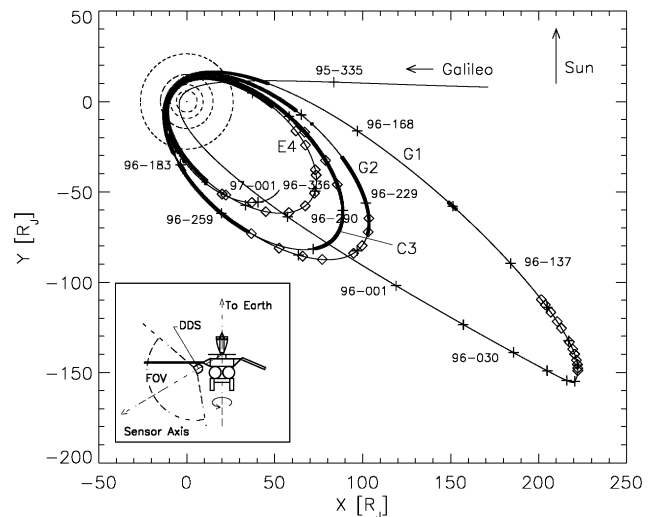

Fig. 1. Galileo's trajectory in the Jovian system in 1996 in a Jupiter-centred coordinate system (thin solid line). Crosses mark the spacecraft position at about 15-day intervals (yy–day). Periods when RTS data were obtained are shown as thick solid lines, MROs are marked by diamonds. Galileo's 1996 orbits are labelled 'G1', 'G2', 'C3' and 'E4'. Sun direction is to the top, and the orbits of the Galilean satellites are indicated (dashed lines). The inset shows a sketch of the Galileo spacecraft with its antenna pointing towards Earth, the dust detector (DDS) and its field of view (FOV). DDS makes about 3 revolutions per minute. Sun and Earth direction coincide to within 10°.

duced from the accumulators are typically averaged over one to several days. Electronic access to the complete data set including the numbers of impacts deduced from the accumulators in full time resolution is also possible via the world wide web: http://www.mpi-hd.mpg.de/dustgroup/.

This paper is organized similarly to our previous papers. Section 2 gives a brief overview of the Galileo mission until the end of 1996, the dust instrument and lists important mission events in 1996. A description of the new Galileo dust data set for 1996 together with a discussion of the detected noise and dust impact rates is given in Section 3. Section 4 analyses and discusses various characteristics of the new data set. Finally, in Section 5 we discuss results of the Jovian dust complex achieved with the new data set.

2. Mission and instrument operations

Galileo was launched on 18 October 1989. Two fly-bys at Earth and one at Venus between 1990 and 1992 gave the spacecraft enough energy to leave the inner solar system. During its interplanetary voyage Galileo had close encounters with the asteroids Gaspra and Ida. On 7 December 1995 the spacecraft arrived at Jupiter and was injected into a highly elliptical orbit about the planet. Galileo's trajectory during its orbital tour about Jupiter from December 1995 to early January 1997 is shown in Fig. 1. Galileo now performs regular close fly-bys of Jupiter's Galilean satellites. Four such encounters occurred in 1996 (two at Ganymede, one at Callisto and one at Europa, see Table 1). Galileo orbits are labelled with the first letter of

Table 1
Galileo mission and dust detector (DDS) configuration, tests and other events[a,b]

Yr–day	Date	Time	Event
89–291	18 Oct 1989	16:52	Galileo launch
95–341	07 Dec 1995	21:54	Galileo Jupiter closest approach, distance: $4.0R_J$
95–341	07 Dec 1995	23:25	DDS configuration: HV = off
96–087	27 Mar 1996	05:56	DDS configuration: HV = 2, EVD = C, I, SSEN = 0, 0, 1, 1
96–089	29 Mar 1996	16:34	DDS first MRO after high-voltage switch on
96	April/May 1996		Galileo reprogramming (phase 2 software)
96–145	24 May 1996	21:00	DDS begin RTS data after Galileo reprogramming
96–153	01 Jun 1996	10:15	DDS end RTS data
96–175	23 Jun 1996	16:17	DDS begin RTS data
96–175	23 Jun 1996	17:04	Galileo turn: $20°$, turn to nominal attitude
96–176	24 Jun 1996	18:30	Galileo OTM-6, duration 5 h, no attitude change
96–179	27 Jun 1996	06:07	DDS end RTS data, begin record data
96–179	27 Jun 1996	06:29	**Galileo Ganymede 1 (G1) closest approach**, altitude 835 km
96–179	27 Jun 1996	06:53	DDS end record data, begin RTS data
96–179	27 Jun 1996	~ 12 h	DDS begin deadtime caused by strong channeltron noise
96–180	28 Jun 1996	00:31	Galileo Jupiter closest approach, distance $11R_J$
96–180	28 Jun 1996	22:48	Galileo turn: $33.4°$, duration 9.1 h
96–181	29 Jun 1999	~ 0 h	DDS end deadtime caused by strong channeltron noise
96–181	29 Jun 1996	06:56	Galileo turn: $28.4°$, duration 42 h
96–182	30 Jun 1996	07:45	Galileo OTM-7A, duration 15 h, no attitude change
96–183	01 Jul 1996	01:03	Galileo turn: $5.1°$, return to nominal attitude
96–183	01 Jul 1996	08:52	DDS end RTS data
96–185	03 Jul 1996	09:00	Galileo OTM-7B, duration 15 h, no attitude change
96–218	05 Aug 1996	08:00	Galileo OTM-8, duration 8 h, size of turn $15°$
96–220	07 Aug 1996	03:28	DDS begin RTS data
96–232	19 Aug 1996	02:18	Galileo turn: $3.8°$, return to nominal attitude
96–237	24 Aug 1996	14:15	Galileo spacecraft anomaly, end of RTS data
96–240	27 Aug 1996	17:30	Galileo OTM-9, duration 5 h, no attitude change
96–244	31 Aug 1996	12:30	DDS begin RTS data after spacecraft anomaly
96–248	04 Sep 1996	18:50	Galileo OTM-10, duration 4.8 h, no attitude change
96–250	06 Sep 1996	11:20	DDS configuration: HV = 2, EVD = I, SSEN = 0, 1, 1, 1, $18R_J$ from Jupiter
96–250	06 Sep 1996	18:32	DDS end RTS data, begin record data
96–250	06 Sep 1996	19:00	**Galileo Ganymede 2 (G2) closest approach**, altitude 262 km
96–250	06 Sep 1996	19:28	DDS end record data, begin RTS data
96–250	06 Sep 1996	20:07	Galileo turn: $23°$, duration 3 h, return to nominal attitude
96–251	07 Sep 1996	13:38	Galileo Jupiter closest approach, distance $10.7R_J$
96–252	08 Sep 1996	16:07	DDS configuration: HV = 2, EVD = C, I, SSEN = 0, 0, 1, 1, $18R_J$ from Jupiter
96–253	09 Sep 1996	21:30	Galileo OTM-11, duration 8 h, size of turn $88°$, return to nominal attitude
96–255	11 Sep 1996	02:39	DDS end RTS data, begin record data
96–255	11 Sep 1996	03:19	DDS end record data, begin RTS data
96–262	18 Sep 1996	16:41	DDS end RTS data
96–267	23 Sep 1996	17:00	Galileo turn: $5°$, new nominal attitude
96–274	30 Sep 1996	23:08	DDS begin RTS data
96–282	08 Oct 1996	14:30	Galileo OTM-12, duration 7.5 h, no attitude change
96–306	01 Nov 1996	13:30	Galileo OTM-13, duration 5 h, no attitude change
96–309	04 Nov 1996	13:15	DDS end RTS data, begin record data
96–309	04 Nov 1996	13:34	**Galileo Callisto 3 (C3) closest approach**, altitude 1136 km
96–309	04 Nov 1996	14:01	DDS end record data, begin RTS data
96–310	05 Nov 1996	10:11	DDS configuration: HV = 2, EVD = I, SSEN = 0, 1, 1, 1, $18R_J$ from Jupiter
96–311	06 Nov 1996	13:31	Galileo Jupiter closest approach, distance $9.2R_J$
96–312	07 Nov 1996	03:10	Galileo turn: $16.2°$, duration 17.5 h, return to nominal attitude
96–312	07 Nov 1996	16:42	DDS configuration: HV = 2, EVD = C, I, SSEN = 0, 0, 1, 1, $18R_J$ from Jupiter
96–313	08 Nov 1996	23:20	Galileo turn: $98.8°$, duration 11 h, return to nominal attitude
96–315	10 Nov 1996	07:20	Galileo OTM-14, no attitude change
96–316	11 Nov 1996	02:01	DDS end RTS data
96–316	11 Nov 1996	20:00	Galileo turn: $5.9°$, new nominal attitude
96–331	26 Nov 1996	11:50	Galileo OTM-15, no attitude change
96–339	04 Dec 1996	16:33	DDS last MRO before reprogramming
96–339	04 Dec 1996	17:00	DDS reprogramming (AC21 and AC31 overflow counters added)
96–340	05 Dec 1996	03:50	DDS first MRO after reprogramming
96–348	13 Dec 1996	19:15	DDS begin RTS data
96–351	16 Dec 1996	02:30	Galileo OTM-16, duration 5 h, no attitude change

Table 1 (*continued*).

Yr–day	Date	Time	Event
96–353	18 Dec 1996	11:00	DDS configuration: HV = 2, EVD = I, SSEN = 0, 1, 1, 1, $18R_J$ from Jupiter
96–354	19 Dec 1996	03:22	Galileo Jupiter closest approach, distance $9.2R_J$
96–354	19 Dec 1996	06:26	DDS end RTS data, begin record data
96–354	19 Dec 1996	06:53	**Galileo Europa 4 (E4) closest approach**, altitude 692 km
96–354	19 Dec 1996	07:24	DDS end record data, begin RTS data
96–355	20 Dec 1996	04:00	Galileo turn: $80.6°$, duration 14.4 h, return to nominal attitude
96–355	20 Dec 1996	06:43	DDS configuration: HV = 2, EVD = C, I, SSEN = 0, 0, 1, 1, $18R_J$ from Jupiter
96–356	21 Dec 1996	19:00	DDS end RTS data
96–358	23 Dec 1996	09:30	Galileo OTM-17, duration 9 h, no attitude change
96–361	26 Dec 1996	20:38	Galileo turn: $11.0°$, new nominal attitude

[a]See text for details. Only selected events are given before 1996. Distances from Jupiter are measured from the center of the planet, altitudes are measured from the surface (Jupiter radius $R_J = 71492$ km).

[b]Abbreviations used: MRO: DDS memory read-out; HV: channeltron high-voltage step; EVD: event definition, ion- (I), channeltron- (C), or electron-channel (E); SSEN: detection thresholds, ICP, CCP, ECP and PCP; OTM: orbit trim maneuver; RTS: Realtime science; AC21: class 2 amplitude range 1 accumulator; AC31: class 3 amplitude range 1 accumulator.
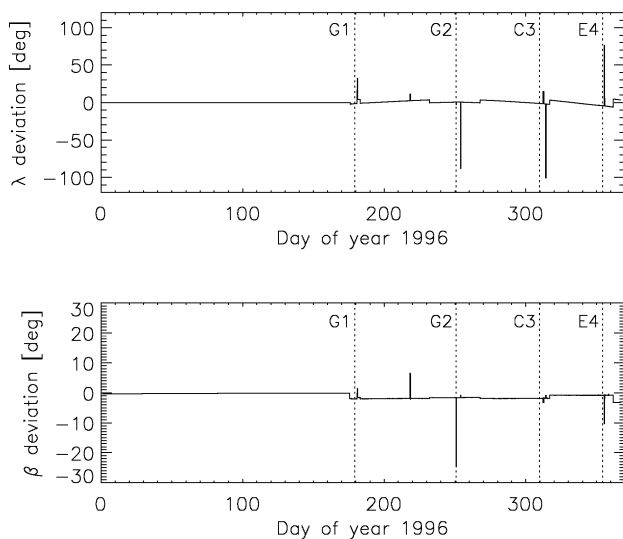

Fig. 2. Spacecraft attitude: deviation of the antenna pointing direction (i.e. negative spin axis) from the Earth direction. The angles are given in ecliptic longitude (top) and latitude (bottom, equinox 1950.0) The four targeted encounters of Galileo with the Galilean satellites are indicated by dotted lines. Sharp spikes are associated with imaging observations with Galileo's cameras or orbit trim maneuvers with the spacecraft thrusters.

the Galilean satellite which was the encounter target during that orbit, followed by the orbit number. For example, "E4" refers to Galileo's fourth orbit about Jupiter which had a close fly-by at Europa. Satellite fly-bys occurred within two days of Jupiter closest approach (pericenter passage). A detailed description of the Galileo mission and the spacecraft have been given by Johnson et al. (1992) and D'Amario et al. (1992).

Galileo is a dual spinning spacecraft with an antenna that points antiparallel to the positive spin axis. During most of the initial 3 years of the mission the antenna pointed towards the Sun (see Paper II). Since 1993 the antenna has usually been pointing towards Earth. Deviations from the

Earth pointing direction in 1996, which is the time period considered in this paper, are shown in Fig. 2. Sharp spikes in the pointing deviation occurred when the spacecraft was turned away from the nominal Earth direction for dedicated imaging observations with Galileo's cameras or for orbit trim maneuvers with the spacecraft thrusters. These spikes lasted typically several hours (see Table 1).

The dust detector system (DDS) is mounted on the spinning section of Galileo and the sensor axis is offset by an angle of $60°$ from the positive spin axis (an angle of $55°$ has been erroneously stated earlier). A schematic view of the Galileo spacecraft and the geometry of dust detection are shown in the inset of Fig. 1 (see also Paper IV and Grün et al., 1998).

The rotation angle measures the viewing direction of the dust sensor at the time of a dust impact. During one spin revolution of the spacecraft the rotation angle scans through a complete circle of $360°$. At rotation angles of $90°$ and $270°$ the sensor axis lies nearly in the ecliptic plane, and at $0°$ it is close to the ecliptic north direction. DDS rotation angles are taken positive around the negative spin axis of the spacecraft. This is done to easily compare Galileo spin angle data with those taken by Ulysses, which, unlike Galileo, has its positive spin axis pointed towards Earth. DDS has a $140°$ wide field of view, although a smaller field of view applies to a subset of dust impacts—the so-called class 3 impacts (Krüger et al., 1999c). During one spin revolution of the spacecraft the sensor axis scans a cone with $120°$ opening angle towards the anti-Earth direction. Dust particles which arrive from within $10°$ of the positive spin axis (anti-Earth direction) can be detected at all rotation angles, whereas those that arrive at angles from $10°$ to $130°$ from the positive spin axis can be detected over only a limited range of rotation angles.

In June 1990 DDS was reprogrammed for the first time after launch and since then the DDS memory can store 46 instrument data frames (with each frame comprising the complete data set of an impact or noise event, consisting of 128

bits, plus ancillary and engineering data; see Papers I and II). DDS time-tags each impact event with an 8-bit word allowing for the identification of 256 unique times. Since 1990 the step size of this time word is 4.3 h. The total accumulation time after which the time word is reset and the time labels of older impact events become ambiguous is $256 \times 4.3\,\text{h} = 46\,\text{days}$.

During most of the interplanetary cruise (i.e. before 7 December 1995) we received DDS data as instrument memory-readouts (MROs). MROs return event data which have accumulated in the instrument memory over time. The contents of all 46 instrument data frames of DDS is transmitted to Earth during an MRO. If too many events occur between two MROs, the data sets of the oldest events become overwritten in the instrument memory and are lost.

Because the high-gain antenna of Galileo did not open completely, the on-board computer of the spacecraft had to be reprogrammed to establish a completely new telecommunications link. New flight-software was installed in the spacecraft computer in April and May 1996 (Statman and Deutsch, 1997), which provided a new mode for high-rate dust data transmission to the Earth, the so-called realtime science mode (RTS). In RTS mode, DDS data were read-out either every 7.1 or every 21.2 min depending on the spacecraft data transmission rate, and were usually directly transmitted to Earth with a rate of 3.4 or 1.1 bits per second, respectively. For short periods (i.e. $\sim \pm 1/2$ h) around satellite closest approaches, DDS data were collected with a higher rate of about 24 bits per second, recorded on the tape recorder (record mode) and transmitted to Earth several days to a few weeks later. Sometimes RTS data for short-time intervals were also stored on the tape recorder and transmitted later but this did not change the labelling—they are called RTS.

In RTS and record mode only seven instrument data frames are read-out at a time and transmitted to Earth rather than the complete instrument memory. Six of the frames contain the information of the six most recent events in each amplitude range (see Paper I and Section 3 for a definition of the amplitude ranges). The seventh frame belongs to an older event read-out from the instrument memory (FN = 7) and is transmitted in addition to the six new events. The position in the instrument memory from which this seventh event is read changes for each read-out so that after 40 read-outs the complete instrument memory gets transmitted (note that the contents of the memory may change significantly during the time period of 40 read-outs if high event rates occur). Although fewer data frames can be read-out this way at a time, the number of new events that can be transmitted to Earth in a given time period is much larger than with MROs because the read-outs occur much more frequently.

In 1996, RTS and record data were obtained during a period of 100 days (Fig. 1). During the remaining times when DDS was operated in neither RTS nor record mode, MROs occurred at several day intervals. Except before 29 March 1996 the MROs were frequent enough so that no ambigu-
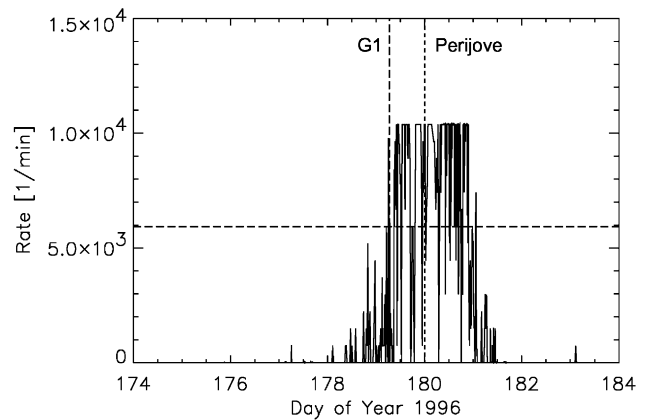
Fig. 3. Channeltron noise rate during the G1 orbit in the inner Jovian system. The noise rate of the smallest class 0 events (AR1, positive signal charge $Q_I < 10^{-13}$ C) plus the noise rate detected by the channeltron noise counter are shown. The dashed horizontal line indicates noise rates above which considerable dead-time occurs. The vertical dashed lines indicate the G1 Ganymede fly-by and perijove passage (perijove distance from Jupiter was $11R_J$).

ities occurred in the time-tagging (i.e. MROs occurred at intervals smaller than 46 days).

Table 1 lists significant mission and dust instrument events for 1996. A comprehensive list of earlier events can be found in Papers II and IV. After Galileo's Io and Jupiter fly-bys on 7 December 1995, the channeltron high voltage of DDS was switched off completely. More than 3 months later, on 27 March 1996, the instrument was reactivated and brought into the same nominal mode with which it was operated during most of Galileo's interplanetary cruise to Jupiter: the channeltron voltage was set to 1020 V (HV = 2), the event definition status was set such that the channeltron or the ion-collector channel can independently initiate a measurement cycle (EVD = C, I) and the detection thresholds for the charges on the ion-collector, channeltron, electron-channel and entrance grid were set (SSEN = 0, 0, 1, 1). This was also the nominal configuration for most of the orbital tour in the Jovian system. Detailed descriptions of the symbols are given in Paper I.

When Galileo performed its first passage through the inner Jovian system after insertion into an orbit about Jupiter (G1 orbit, June 1996) DDS was operated in its nominal mode as described above. This was also the mode DDS was operated in during Galileo's 6-year interplanetary cruise. In this mode high channeltron noise rates were recorded within about $20R_J$ distance from Jupiter (Jupiter radius, $R_J = 71,492\,\text{km}$) which reached values of up to 10,000 events per minute (Fig. 3). Because the time the onboard computer of DDS needs to process data from a single event (impact or noise) is about 10 ms (Grün et al., 1995c), significant dead time is produced when the event rate exceeds 6000 min^{-1}. Hence, only very few dust impacts could be recorded from day 179.5 to 181.0 in 1996. During all later orbits of Galileo's prime Jupiter mission the event definition status and the detection

threshold for the channeltron charge were changed within $18R_J$ (see Table 1). This reduced the noise sensitivity in the inner Jovian system and effectively prevented dead-time problems in the G2 and all later orbits.

During the Jupiter orbital tour of Galileo, orbit trim maneuvers (OTMs) have been executed around perijove or apojove passages to target the spacecraft to close encounters with the Galilean satellites. A few of these maneuvers required changes in the spacecraft attitude off the nominal Earth pointing direction (see Fig. 2). In one case, on 9 September 1996, the spacecraft was turned by $88°$. In addition, dedicated spacecraft turns occurred typically in the inner Jovian system within a few days around perijove to allow for imaging observations with Galileo's cameras or to maintain the nominal Earth pointing direction. A large turn by $99°$ off the Earth direction occurred on 8 November 1996. Both attitude changes on 9 September and 8 November were large enough that DDS could record impacts of dust stream particles at times when these particles would have been undetectable with the nominal spacecraft orientation (Grün et al., 1998)

A spacecraft anomaly occurred on 24 August 1996 and no dust data were obtained until 31 August when the spacecraft was recovered. Although the dust instrument continued to collect data they could not be transmitted to Earth and most of them were lost. The data set for only 5 grains detected in this time period was transmitted as data read from the instrument memory (FN = 7).

DDS classifies and counts all registered events with 24 dedicated accumulators (see Section 3 and Paper I). During Galileo's first orbits about Jupiter (G1, G2 and C3) unanticipated high rates occurred in two of the highest quality categories and unrecognized accumulator overflows may have occurred. To detect such overflows, DDS was reprogrammed on 4 December 1996 by adding two overflow counters. The details of this reprogramming and the significance of possible accumulator overflows are described in Section 3.

3. Impact events

DDS classifies all events—real impacts of dust particles and noise events—into one of 24 different categories (6 amplitude ranges for the charge measured on the ion collector grid and 4 event classes) and counts them in 24 corresponding 8-bit accumulators (Paper I). In interplanetary space most of the 24 categories described above were relatively free from noise and only sensitive to real dust impacts, except for extreme situations like the crossings of the radiation belts of Earth, Venus (Paper II) and Jupiter (Paper IV). During most of Galileo's initial 3 years of interplanetary cruise only the lowest amplitude and class categories—AC01 (event class 0, amplitude range 1, AR1), AC11, and AC02—were contaminated by noise events (Paper II). In July 1994 the onboard classification scheme of DDS was changed to identify smaller dust impacts in the data. With the modified scheme noise events were usually restricted to class 0 but may have occurred in all amplitude ranges. All events in higher quality classes detected in the low radiation environment of interplanetary space were true dust impacts (class 0 may still contain unrecognized dust impacts).

In the extreme radiation environment of the Jovian system, a different noise behaviour of the instrument was recognized: especially when Galileo was within about $20R_J$ from Jupiter the higher event classes were contaminated by noise (see also Paper IV). This noise, which affects classes 1 and 2, is unrelated to the channeltron noise shown in Fig. 3. In an analysis of the whole dust data set from Galileo's prime Jupiter mission, noise events could be eliminated from class 2 (Krüger et al., 1999c). Class 1 events, however, show signatures of being nearly all noise events in the Jovian environment. We therefore consider the class 3 and the denoised class 2 impacts as the complete set of dust data from Galileo's Jupiter tour. Apart from a missing third charge signal—class 3 has three charge signals and class 2 only two—there is no physical difference between dust impacts categorized into class 2 or class 3.

In this paper the terms "small" and "big" have the same meaning as in Paper IV (which is different from the terminology of Paper II). We call all particles in class 2 and class 3 in the amplitude ranges 2 and higher (AR2 to AR6) "big". Particles in the lowest amplitude range (AR1) are called "small". This distinction separates the small Jovian dust stream particles from bigger grains which are mostly detected between and near the Galilean satellites.

In RTS and record mode the time between two readouts of the instrument memory determines the number of events in a given time period for which their complete information can be transmitted. Thus, the complete information on each impact is transmitted to Earth when the impact rate is below one impact per either 7.1 or 21.2 min in RTS mode or one impact per minute in record mode. If the impact rate exceeds these values, the detailed information of older events is lost because the full data set of only the latest event is stored in the DDS memory.

Furthermore, in these two modes the time between two read-outs also limits the accuracy with which the impact time can be determined. It is 7.1 or 21.2 min in RTS mode and about 1 min in record mode, respectively. During times when only MROs occurred, the accuracy is limited by the increment of the DDS internal clock, i.e. 4.3 h.

Because of the large differences in the timing accuracy in the various read-out modes, we have defined a new parameter, time error value—TEV, that determines the accuracy of the impact time of a dust particle in minutes. TEV has been rounded to the next higher integer. In RTS and record mode, TEV is usually simply the time between two read-outs, i.e. TEV = 8 or 22 min in RTS or TEV = 2 min in record mode, respectively. During gaps in the data transmission, i.e. when data packets were lost, multiples of these values occur. Usually, the given impact time of a dust particle is identical with the readout time of the instrument, which means that the

impact has occurred some time in the period impact time minus TEV. This is the case for almost all impacts in AR2 to AR6 and more than 70% of the impacts in AR1. For example the impact of particle 3497 in Table 5 (TEV = 8 min) occurred between 96-180 10:06 and 96-180 10:14.

Data frames belonging to older events not transmitted immediately after impact but transmitted later (as the seventh event from each read-out, FN = 7) have impact times interpolated to lie between the times of the two adjacent read-outs. Their TEV value is equal to the time interval between these adjacent read-outs. For MROs the impact time has been interpolated to the middle of the time interval defined by the DDS internal clock. The corresponding TEV is 259 min $\sim$ 4.3 h. For example, impact 3780 in Table 5 (TEV = 259 min) occurred at 96-241 23 : 55 $\pm$ 259/2 min.

DDS records and counts the number of all dust particle impacts and noise events with 8 bit accumulators. The time between two readouts of the instrument memory determines the maximum rate which can unambiguously be derived from the accumulators. At rates below $256/7.1 \sim 36\ \mathrm{min}^{-1}$ or $256/21.2 \sim 12\ \mathrm{min}^{-1}$ in RTS mode and below $\sim 200\ \mathrm{min}^{-1}$ in record mode the accumulator values transmitted to Earth represent the true event rates. During times of higher event rates an unknown number of accumulator overflows occurred which led to ambiguities in the number of events derived from the accumulators. Thus, the derived rates may be underestimated.

To cope with unanticipated high rates in the inner Jovian system (see Fig. 4 and Grün et al., 1998) DDS was reprogrammed on 4 December 1996. Two of the 24 accumulators (AC05 and AC06) were modified to count the number of accumulator overflows of the two highest quality classes in the lowest amplitude range (AC21 and AC31). Since then the maximum recordable rate in RTS mode is $256^2/7.1 \sim 9000\ \mathrm{min}^{-1}$ or $256^2/21.2 \sim 3000\ \mathrm{min}^{-1}$, depending on the readout interval, and about $25{,}000\ \mathrm{min}^{-1}$ in record mode. These rates have never been exceeded since the DDS reprogramming.

The collection of data mostly relied on MROs when DDS detected relatively low impact and noise rates. The timing accuracy of these events, however, is less precise (TEV = 259).

Table 2 lists the number of all dust impacts and noise events identified with the Galileo dust sensor in 1996 as deduced from the accumulators of classes 2 and 3. Depending on the event rate, the numbers are given in intervals from half a day to a few weeks (the numbers with the highest time resolution achievable are available in electronic form only and are provided to the data archiving centers). For these two classes with the lowest amplitude range AR1 the complete data set for only 2% of the detected events was transmitted, the remaining 98% of events were only counted. Nearly all data sets for events in higher amplitude ranges were transmitted, although a few were also lost in AR2 and AR3. We give only the number of events in classes 2 and 3 because they have been shown to contain real dust impacts: class 3 is
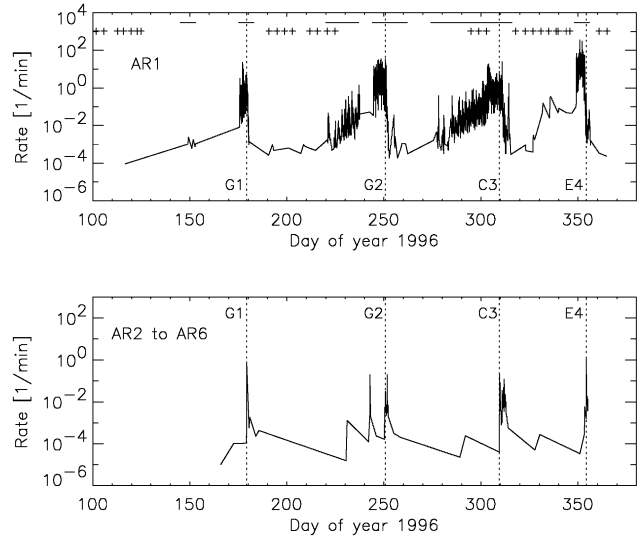
Fig. 4. Dust impact rate detected by DDS in 1996. The upper panel shows the impact rate in AR1 which represents the Io dust streams, the lower panel that for the higher amplitude ranges AR2 to AR6. Dotted lines indicate the closest approaches to the Galilean satellites. Perijove passages occurred within 2 days of the satellite closest approaches. These curves are plotted from the number of impacts with the highest time resolution which is available only in electronic form. No smoothing has been applied which leads to the 'sawtooth' pattern, especially prominent in the lower panel. In the upper panel, time intervals with continuous RTS data coverage are indicated by horizontal bars, memory readouts (MROs) are marked by crosses.

practically noise free (although Krüger et al., 1999c found indications for a very small number of noise events in class 3, AR1, in the inner Jovian system). Class 2 is strongly contaminated by noise events in the inner Jovian system (within about $20R_\mathrm{J}$ from Jupiter).

The data set we present here has been denoised according to the criteria derived by Krüger et al. (1999c). The noise contamination factor f_noi for class 2 listed in Table 2 for the six different amplitude ranges has been derived with two different methods: for AR1 we use the procedure described by (Krüger et al., 1999c), i.e. a 1-day average of the ratio between the number of class 2 AR1 noise events and the total number of class 2 AR1 events (noise plus dust) for which the full data set is available. This defines the scaling factor f_noi with which the number of AC21 of events derived has to be multiplied in order to get the number of noise events from the AC21 accumulator. It should be noted that the criteria applied to identify noise events in the DDS data have been derived with our present knowledge of the instrument behaviour in the Jovian environment. Future analyses may lead to an improved picture of the noise characteristics and to modified algorithms for noise rejection.

For the higher amplitude ranges AR2 to AR6 the full data set is available for most detected events. Thus, from the charge amplitudes and rise times we can determine for each accumulator increment listed in Table 2 whether it was due to a noise event or a dust impact. During time intervals

Table 2
Overview of dust impacts accumulated with Galileo DDS between 1 January and 31 December 1996[a]

Date	Time	D_{Jup} (R_J)	Δt (d)	$f_{noi,AC21}$	AC 21[b]	AC 31[b]	$f_{noi,AC22}$	AC 22	AC 32	$f_{noi,AC23}$	AC 23	AC 33	$f_{noi,AC24}$	AC 24	AC 34	$f_{noi,AC25}$	AC 25	AC 35	$f_{noi,AC26}$	AC 26	AC 36
96–148	11:14	175.5	151.9	0.80	5	—	—	—	—	—	—	1	—	—	—	—	—	—	—	—	—
96–165	23:03	107.9	17.49	0.27	11	—	0.00	1	1	—	—	—	—	—	—	—	—	—	—	—	—
96–176	00:03	45.10	10.04	0.17	134	269	0.00	1	—	—	—	—	—	—	—	—	—	—	—	—	—
96–177	00:50	36.22	1.032	0.00	304	64	—	—	—	—	—	—	—	—	—	—	—	—	—	—	—
96–178	14:13	21.40	1.558	0.02	4133	938	1.00	1	—	—	—	—	—	—	—	—	—	—	—	—	—
96–179	03:19	16.18	0.545	0.12	972	31	0.00	1	—	—	—	—	—	—	—	—	—	—	—	—	—
96–180	10:14	12.38	1.288	0.30	1398	29	0.50	2	2	—	—	—	—	—	—	—	—	—	—	—	—
96–181	00:16	17.14	0.584	1.00	37	—	1.00	3[b]	—	0.00	1	—	—	—	—	—	—	—	—	—	—
96–182	00:20	26.55	1.002	1.00	3	—	—	—	—	—	—	—	—	—	—	—	—	—	—	—	—
96–185	13:18	53.60	3.540	1.00	1	—	0.50	2	—	—	—	—	—	—	1	—	—	—	—	—	—
96–194	04:23	94.16	8.628	0.74	15	—	1.00	2	—	—	—	—	—	—	—	—	—	—	—	—	—
96–209	11:05	125.3	15.27	0.74	17	—	1.00	1	—	—	—	—	—	—	—	—	—	—	—	—	—
96–221	14:51	125.7	12.15	0.77	30	—	1.00	1	—	—	—	—	—	—	—	—	—	—	—	—	—
96–231	00:38	111.9	9.407	0.32	91	5	1.00	1	—	—	—	2	—	—	—	—	—	—	—	—	—
96–241	23:55	75.75	10.97	0.07	444	73	1.00	25[b]	1	—	—	—	—	—	—	—	—	—	—	—	—
96–242	17:05	72.30	0.715	0.12	246	173	0.67	3[b]	—	—	—	—	—	—	—	—	—	—	—	—	—
96–245	00:11	59.93	2.295	0.00	2595	666	0.00	2	—	—	—	—	—	—	—	—	—	—	—	—	—
96–246	00:36	53.67	1.017	0.04	5091	1202	1.00	1	—	—	—	—	—	—	—	—	—	—	—	—	—
96–247	00:05	47.11	0.978	0.03	4436	1139	—	—	—	—	—	—	—	—	—	—	—	—	—	—	—
96–247	21:19	40.62	0.884	0.03	4897	1392	1.00	1	—	—	—	—	—	—	—	—	—	—	—	—	—
96–248	00:01	39.75	0.113	0.00	765	168	—	—	—	—	—	—	—	—	—	—	—	—	—	—	—
96–249	00:10	31.52	1.005	0.00	8443	2358	—	—	—	—	—	—	—	—	—	—	—	—	—	—	—
96–250	06:53	19.74	1.279	0.05	8849	1213	—	—	1	—	—	—	—	—	—	—	—	—	—	—	—
96–251	02:47	12.38	0.829	0.25	6314	400	0.75	4	1	—	—	2	0.00	1	1	—	—	1	—	—	—
96–252	07:27	14.69	1.194	0.50	891	108	0.14	7	—	0.00	1	1	—	—	1	—	—	—	—	—	—
96–255	01:49	38.94	2.765	0.97	14	—	0.67	3	—	—	—	—	—	—	2	—	—	—	—	—	—
96–260	19:33	72.31	5.739	0.97	77	83	1.00	1	—	—	—	—	—	—	1	—	—	—	—	—	—
96–270	22:28	103.2	10.12	0.67	3	—	1.00	1	—	—	—	—	—	—	—	—	—	—	—	—	—
96–285	16:03	111.5	14.73	0.25	147	1	1.00	1	—	—	—	—	—	—	—	—	—	—	—	—	—
96–291	23:09	103.6	6.296	0.23	194	2	1.00	1	1	—	—	—	—	—	—	—	—	—	—	—	—
96–305	00:16	58.77	13.04	0.01	8485	3324	—	—	—	—	—	—	—	—	—	—	—	—	—	—	—
96–306	00:03	52.93	0.991	0.07	1607	184	—	—	—	—	—	—	—	—	—	—	—	—	—	—	—
96–307	00:07	46.43	1.002	0.00	1324	178	—	—	—	—	—	—	—	—	—	—	—	—	—	—	—
96–308	08:12	36.63	1.336	0.01	2520	405	1.00	1	—	—	—	—	—	—	—	—	—	—	—	—	—
96–309	09:06	27.92	1.037	0.04	1154	199	0.00	1	—	—	—	—	—	—	—	—	—	—	—	—	—

Date	Time	D_{Jup}	Δt	f_{noi}	C2	C3	f_{noi}	AC22	AC32	f_{noi}	AC23	AC33	f_{noi}	AC24	AC34	f_{noi}	AC25	AC35	f_{noi}	AC26	AC36
96–310	04:59	20.16	0.828	0.07	1480	98	—	—	2	—	—	—	—	—	—	—	—	—	—	—	—
96–311	00:12	12.25	0.801	0.25	2838	166	0.00	1	1	0.00	1	—	—	—	—	—	—	—	—	—	—
96–312	01:13	11.65	1.042	0.74	466	41	0.71	7[b]	2	0.00	2[b]	2	0.00	1	—	—	1	—	—	—	—
96–314	00:45	30.37	1.980	0.92	119	5	0.54	13[b]	—	1.00	1[b]	2	0.00	1	—	—	1	1	—	—	—
96–327	17:44	85.63	13.70	0.38	358	54	0.00	1	—	—	—	—	—	—	—	—	—	—	—	—	—
96–330	06:08	88.24	2.516	0.75	14	1	—	—	—	—	—	—	—	—	—	—	1	—	—	—	—
96–339	16:35	82.84	9.435	0.00	861	68	—	—	—	—	—	—	—	—	—	—	—	—	—	—	—
96–339	17:00	82.80	0.017	—	—	—	—	—	—	—	—	—	—	—	—	—	—	—	—	—	—
96–349	00:17	49.16	9.321	0.00	384	127	—	—	—	—	—	—	—	—	—	—	—	—	—	—	—
96–350	20:31	36.91	1.843	0.00	50323[c]	9994[c]	0.00	1[b]	—	—	—	—	—	—	—	—	—	—	—	—	—
96–350	22:38	36.25	0.088	0.00	17091[c]	1791[c]	0.00	1[b]	—	—	—	—	—	—	—	—	—	—	—	—	—
96–351	00:24	35.69	0.073	0.00	455[c]	85[c]	—	—	—	—	—	—	—	—	—	—	—	—	—	—	—
96–352	23:57	18.08	1.980	0.05	81422[c]	10383[c]	—	—	—	—	—	—	—	—	—	—	—	—	—	—	—
96–353	06:33	15.29	0.275	0.23	1133[c]	65[c]	—	—	1	—	—	—	—	—	—	—	—	—	—	—	—
96–354	06:27	9.370	0.995	0.48	5957[c]	436[c]	0.50	2	1	0.00	2	—	—	—	—	—	—	—	—	—	—
96–355	00:47	15.55	0.763	0.96	104[c]	3[c]	0.33	15[b]	2	0.00	1	1	0.00	1	—	—	1	—	—	—	—
96–360	19:31	54.22	5.780	0.74	67[c]	2[c]	1.00	4	—	—	—	—	—	—	—	—	—	—	—	—	—
96–365	04:07	67.34	4.358	0.88	11[c]	—	—	—	—	—	—	—	—	—	—	—	—	—	—	—	—
Events (counted)				—	228730[d]	37923[d]	—	113	16	—	9	11	—	4	7	—	2	3	—	0	—
Impacts (complete data)				—	1807	3451	—	39	16	—	8	11	—	6	7	—	3	3	—	2	—
All events(complete data)				0.28	2512	3451	0.53	83	16	0.20	10	11	0.00	6	7	0.00	3	3	0.00	2	—

[a] The Jovicentric distance D_{Jup}, the lengths of the time interval Δt (days) from the previous table entry, and the corresponding numbers of impacts are given for the classes 2 and 3 accumulators. The accumulators are arranged with increasing signal amplitude ranges (AR), e.g. AC31 means counter for CLN = 3 and AR = 1. The determination of the noise contamination f_{noi} in class 2 is described in the text. The Δt in the first line (day 96–148) is the time interval counted from the last entry in Table 4 in Paper IV. The DDS reprogramming on day 96–339 is indicated by horizontal lines. The totals of counted impacts, of impacts with complete data, and of all events (noise plus impact events) for the entire period are given as well.

[b] AR2–AR6: The complete data set was transmitted for only a fraction of all particles detected in this amplitude range and time interval. f_{noi} has been estimated from the data sets transmitted. AR1:data transmission is always incomplete in this amplitude range.

[c] After day 96–348 accumulator overflows are fully taken into account and the numbers given are the true numbers of detected events.

[d] Due to an unknown number of accumulator overflows before day 96–339 these numbers are lower limits for the true numbers of events.

Table 3
Criteria for the identification of secondary ejecta grains in the data set

Satellite	Orbit	Rotation angle range	Impact velocity	Class 2 denoised	Altitude limit (km)
Ganymede	G1, G2	$180° \leqslant \text{ROT} \leqslant 360°$	Not restricted	No	39,525
Callisto	C3	$180° \leqslant \text{ROT} \leqslant 360°$	$v \leqslant 10 \text{ km s}^{-1}$	No	48,180
Europa	E4	$180° \leqslant \text{ROT} \leqslant 360°$	Not restricted	Yes	23,400

when the complete data set for some but not all detected events was transmitted, f_{noi} has been calculated from those events for which the full data set is available and it has been assumed that this noise ratio applies to all events detected (i.e. also counted) in this time interval.

It should be noted that the noise identification criteria used here are exactly those derived in (Krüger et al., 1999c). The analysis of the latest data after 1997 has shown that the noise behaviour of the dust sensor has changed due to instrument ageing (see Section 4). Different noise identification criteria have to be applied to later data. Data from 1996 published in this paper are not affected.

The noise identification criteria of Krüger et al. (1999c) which have been applied to the 1996 data have been developed to separate the tiny Jupiter stream particles from noise events. However, they do not work very well to distinguish secondary ejecta grains detected during close satellite fly-bys from noise events. We therefore applied a different technique to identify ejecta grains which is summarized in Tables 3 and 4.

During all four satellite fly-bys in 1996 the detection geometry was such that ejecta grains could be detected from rotation angles $180° \leqslant \text{ROT} \leqslant 360°$ only. During the fly-bys G1, G2 and E4 the impact direction (ROT) could be used as a good parameter to identify ejecta grains because stream particles and ejecta grains approached from opposite directions (Krüger et al., 1999e). During the C3 fly-by, however, the stream particles approached from the same direction as the ejecta grains and the measured impact velocities of the dust particles had to be used as an additional parameter to identify the ejecta (Krüger et al., 2000). The C3 fly-by velocity of Galileo was 8.0 km s^{-1} and we included only particles with a measured impact velocity below 10.0 km s^{-1} in the data set. For the Ganymede and Europa fly-bys we did not limit the velocity range of the grains.

For all four satellite fly-bys of 1996 we included only particles within the approximate Hill radius of the satellite, except for Europa where we used a larger altitude limit because the present data analysis indicates that this dust cloud may be more extended. Denoising has been shown to be important for class 2 in the inner Jovian system (Krüger et al., 1999c), i.e. within about $15R_J$ from Jupiter. We therefore denoised the data from the Europa fly-by but did not denoise the data from the Ganymede and Callisto fly-bys. For denoising of the Europa data we used a slightly different noise separation scheme than Krüger et al. (1999c). Events

Table 4
Criteria to identify noise events in class 2 during the E4 fly-by. Noise events in the lowest amplitude range (AR1) fulfill at least one of the criteria listed below (see Paper I for a definition of the parameters), whereas noise events in the higher amplitude ranges fulfil all criteria listed for AR2 to AR6

Charge parameter	AR1	AR2–AR6
Entrance grid amplitude	$\text{PA} \geqslant 9$	—
Channeltron amplitude	—	$\text{CA} \leqslant 2$
Target amplitude minus iongrid amplitude	$(\text{EA} - \text{IA}) \leqslant 0$ or	$(\text{EA} - \text{IA}) \leqslant 0$ or
	$(\text{EA} - \text{IA}) \geqslant 7$	$(\text{EA} - \text{IA}) \geqslant 7$
EA risetime	$\text{ET} \leqslant 9$ or $\text{ET} = 15$	—
IA risetime	$\text{IT} \leqslant 8$	—

which fulfil the criteria listed in Table 4 have been rejected as noise.

During the first three passages through the inner Jovian system (G1, G2 and C3) an unknown number of accumulator overflows occurred in the lowest amplitude range, especially in class 2. Therefore, the numbers before the instrument reprogramming on 4 December 1996 given in Table 2 should be treated as lower limits, specifically when the corresponding rates are close to the maximum recordable rates described above. For numbers after 13 December 1996 (when the instrument was read out in RTS mode) overflows of the AC21 and AC31 accumulators are fully taken into account and the numbers given in Table 2 represent the true numbers of detected events. Between 4 and 13 December accumulator overflows are also taken into account but due to high dust impact rate and the instrument readout mode with memory readouts occurring at a few day intervals unrecognized overflows may also have happened. Thus, in this time interval impact rates should also be treated with caution.

To our present understanding the lower quality classes 0 and 1 contain only noise events and are therefore not considered here. Future efforts, however, may also lead to the identification of some dust impacts in these low quality classes.

The dust impact rate recorded by DDS in 1996 as deduced from the classes 2 and 3 accumulators is shown in Fig. 4. The impact rate measured in the lowest amplitude range (AR1) and the one measured in the higher amplitude ranges (AR2 to AR6) are shown separately because they reflect two distinct populations of dust. AR1 contains mostly stream particles which have been measured throughout the Jovian

system. Bigger particles (AR2 to AR6) have been mostly detected between the Galilean satellites. This is illustrated in the diagram: the impact rate for AR1 gradually increases when Galileo approaches the inner Jovian system, whereas it shows narrow peaks close to the perijove passages in the case of the bigger (AR2–AR6) impacts. Diagrams showing the class 3 AR1 impact rate with a much higher time resolution and as a function of distance from Jupiter have been published by Grün et al. (1998) and are not repeated here.

The impact rates of AR1 particles measured in the inner Jovian system reached maximum values of about 20 min^{-1} during the G1, G2, and C3 orbits. These values are close to the saturation limit caused by unrecognized accumulator overflows (see above) and higher short-time peaks may have occurred. More than 100 impacts per minute have been detected in E4 (1996, day 350) which represents the highest impact rate recorded during Galileo's prime mission. Such a high rate could only be recorded in RTS mode after the reprogramming on 4 December 1996.

Table 5 lists the data sets for all 95 big particles detected in classes 2 and 3 between January and December 1996 for which the complete information exists. Class 2 particles have been separated from noise by applying the criteria developed by Krüger et al. (1999c) except for the satellite fly-bys (see above). We do not list the small stream particles (AR1) in Table 3 because their masses and velocities are outside the calibrated range of DDS and they are by far too abundant to be listed here (secondary ejecta grains in AR1 are also omitted). The complete information of a total of 5258 small dust particles has been transmitted in 1996. The stream particles are believed to be about 10 nm in size and their velocities exceed 200 km s^{-1} (Zook et al., 1996). Any masses and velocities derived for these particles with existing calibration algorithms would be unreliable. The full data set for all 5353 small and big particles is submitted to the data archiving centers and is available in electronic form. A total number of 9119 events (dust plus noise in all amplitude ranges and classes) were transmitted in 1996, each with a complete data set.

In Table 5 dust particles are identified by their sequence number and their impact time. Gaps in the sequence number are due to the omission of the small particles. The time error value (TEV) as defined above is listed next. Then the event category—class (CLN) and amplitude range (AR)—are given. Raw data as transmitted to Earth are displayed in the next columns: sector value (SEC) which is the spacecraft spin orientation at the time of impact, impact charge numbers (IA, EA, CA) and rise times (IT, ET), time difference and coincidence of electron and ion signals (EIT, EIC), coincidence of ion and channeltron signal (IIC), charge reading at the entrance grid (PA) and time (PET) between this signal and the impact. Then the instrument configuration is given: event definition (EVD), charge sensing thresholds (ICP, ECP, CCP, PCP) and channeltron high voltage step (HV). See Paper I for further explanation of the instrument parameters, except TEV which is introduced above.

The next four columns in Table 3 give information about Galileo's orbit: ecliptic longitude and latitude (LON, LAT) and distance from Jupiter (D_{Jup}, in R_J). The next column gives the rotation angle (ROT) as described in Section 2. Whenever this value is unknown, ROT is arbitrarily set to 999. This occurs 10 times in the full data set that includes the small particles. Then follows the pointing direction of DDS at the time of particle impact in ecliptic longitude and latitude (S_{LON}, S_{LAT}). When ROT is not valid S_{LON} and S_{LAT} are also useless. Mean impact velocity (v) and velocity error factor (VEF, i.e. multiply or divide stated velocity by VEF to obtain upper or lower limits) as well as mean particle mass (m) and mass error factor (MEF) are given in the last columns. For VEF > 6, both velocity and mass values should be discarded. This occurs for 8 impacts. No intrinsic dust charge values are given (Svestka et al., 1996).

Entries for the parameter PA in Table 3 sometimes have values between 49 and 63 although the highest possible value is 48 (Paper I). This is also inherent in all Galileo and Ulysses data sets published earlier (Papers II–V) and it is due to a bit flip. According to our present understanding the correct PA values are obtained by subtracting 32 from all entries which have values between 49 and 63. Values of 48 and lower should remain unchanged.

4. Analysis

The positive charge measured on the ion collector, Q_I, is the most important impact parameter determined by DDS because it is rather insensitive to noise. Fig. 5 shows the distribution of Q_I for the full 1996 data set (small and big particles together). Ion impact charges have been detected over the entire range of six orders of magnitude the instrument can measure. One impact (or about 0.02% of the total) is close to the saturation limit of $Q_I \sim 10^{-8}$C and may thus constitute a lower limit of the actual impact charge. The impact charge distribution of the big particles ($Q_I > 10^{-13}$C) follows a power law with index -0.31 and is shown as a dashed line. This slope is close to the value of $-1/3$ given for Galileo in Paper II for the inner solar system. It is flatter than the $-1/2$ given for Ulysses in Paper III and the -0.43 given for Galileo in Paper IV, which both mainly reflect the outer solar system. The slopes indicate that, on average, bigger particles have been detected in the inner solar system and in the Jovian system than in the interplanetary space of the outer solar system. This is in agreement with a smaller relative contribution of interstellar particles in the inner solar system and in the Jovian system. Note that the Jovian stream particles (AR1) have been excluded from the power law fit.

In Fig. 5 the small stream particles ($Q_I < 10^{-13}$C) are collected in two histogram bins. Their number per individual digital step is shown separately in Fig. 6 to analyse their behaviour in more detail. The distribution flattens for impact charges below 3×10^{-14}C. This indicates that the sensitivity

Table 5

DPF data: No., impact time, TEV CLN, AR, SEC, IA, EA, CA, IT, ET, EIT, EIC, ICC, PA, PET, EVD, ICP, ECP, CCP, PCP, HV and evaluated data: LON, LAT, D_{Jup} (in R_J; Jupiter radius $R_J = 71492$ km), rotation angle (ROT), instr. pointing (S_{LON}, S_{LAT}), speed (v, in km s^{-1}), speed error factor (VEF), mass (m, in grams) and mass error factor (MEF)

No.	IMP. DATE		TEV	CLN	AR	SEC	IA	EA	CA	IT	ET	EIT	EIC	ICC	PA	PET	EVD	ICP	ECP	CCP	PCP	HV	LON	LAT	D_{Jup}	ROT	S_{LON}	S_{LAT}	V	VEF	M	MEF
2884	96–098	17:36:21	259	3	3	54	20	24	5	6	4	6	0	1	44	0	1	0	1	0	1	2	276.0	0.0	262.424	14	271	52	36.5	1.6	2.0×10^{-13}	6.0
2887	96–148	11:14:13	22	3	2	34	13	21	2	9	4	6	0	1	41	0	1	0	1	0	1	2	279.8	−0.1	175.563	42	296	37	12.7	1.9	2.2×10^{-12}	10.5
2889	96–148	23:52:33	22	2	2	5	8	12	0	9	10	8	0	0	36	0	1	0	1	0	1	2	279.8	−0.1	173.949	83	307	6	18.3	1.6	1.1×10^{-13}	6.0
2897	96–165	23:03:47	259	2	2	166	11	11	4	10	11	0	1	1	3	31	1	0	1	0	1	2	281.0	−0.1	107.912	217	212	−40	9.7	1.9	8.5×10^{-13}	10.5
3367	96–178	14:13:39	22	2	2	112	13	19	18	15	15	0	1	1	38	29	1	0	1	0	1	2	281.5	0.0	21.388	293	229	17	2.5	1.6	2.1×10^{-10}	6.0
3419	96–179	04:23:00	22	2	2	94	8	13	1	11	13	12	0	0	19	24	1	0	1	0	1	2	281.5	0.0	15.774	318	239	36	7.4	1.6	1.5×10^{-12}	6.0
3447	96–179	06:28:55	6	3	2	128	8	12	14	13	14	8	0	1	39	31	1	0	1	0	1	2	281.5	0.0	15.016	270	227	0	2.7	1.6	3.4×10^{-11}	6.0
3450	96–179	06:31:39	2	3	2	150	8	11	4	12	13	6	0	1	4	30	1	0	1	0	1	2	281.5	0.0	14.999	239	230	−25	5.9	1.6	2.3×10^{-12}	6.0
3497	96–180	10:14:41	8	2	3	168	20	21	15	7	9	7	0	1	37	0	1	0	1	0	1	2	281.5	0.0	12.378	214	242	−44	12.7	1.9	4.7×10^{-12}	10.3
3498	96–180	15:47:20	8	2	4	254	24	23	18	13	14	0	1	1	47	16	1	0	1	0	1	2	281.6	0.0	14.042	93	337	−2	2.0	1.9	4.9×10^{-09}	10.5
3499	96–180	20:58:46	8	2	3	113	19	25	5	8	15	8	0	1	23	0	1	0	1	0	1	2	281.6	0.0	15.893	291	229	16	5.6	1.6	8.6×10^{-11}	6.0
3500	96–181	00:16:56	22	2	4	178	28	30	28	11	12	8	0	1	20	0	1	0	1	0	1	2	281.6	0.0	17.150	200	255	−51	2.7	1.6	7.3×10^{-09}	6.0
3501	96–183	22:29:07	259	3	4	18	25	29	22	11	10	6	0	1	47	0	1	0	1	0	1	2	281.9	−0.1	42.430	65	333	19	5.2	1.9	4.9×10^{-10}	10.3
3502	96–184	02:47:58	259	2	2	26	8	12	0	8	0	12	0	0	0	0	1	0	1	0	1	2	281.9	−0.1	43.758	53	330	28	19.0	1.9	9.1×10^{-14}	10.5
3575	96–230	11:32:35	22	3	3	74	22	27	28	4	4	5	0	1	47	0	1	0	1	0	1	2	286.3	−0.2	113.162	346	263	51	52.6	1.6	9.8×10^{-14}	6.0
3581	96–231	00:38:13	22	3	3	139	20	23	1	6	4	7	0	1	44	0	1	0	1	0	1	2	286.3	−0.2	111.990	255	227	−13	36.5	1.6	1.7×10^{-13}	6.0
3780	96–241	23:55:26	259	3	2	180	8	4	17	8	14	11	0	1	8	31	1	0	1	0	1	2	287.1	−0.2	75.744	197	254	−52	19.0	1.9	2.5×10^{-14}	10.5
3782	96–242	17:05:45	259	2	2	145	15	5	6	0	0	9	0	0	0	0	1	0	1	0	1	2	287.2	−0.2	72.299	246	225	−19	11.8	11.8	3.6×10^{-13}	5858.3
3783	96–242	17:10:49	259	2	2	70	8	9	9	8	10	3	1	1	4	31	1	0	1	0	1	2	287.2	−0.2	72.281	352	266	52	19.0	1.9	5.6×10^{-14}	10.5
3784	96–243	01:48:30	259	2	2	74	8	9	9	8	10	3	1	1	6	31	1	0	1	0	1	2	287.2	−0.2	70.481	346	259	51	19.0	1.9	5.6×10^{-14}	10.5
5194	96–250	06:53:06	8	3	2	107	8	12	8	9	9	5	0	1	36	0	1	0	1	0	1	2	287.5	−0.2	19.729	300	227	23	19.9	1.6	7.4×10^{-14}	6.0
5261	96–250	13:29:28	8	3	4	125	25	29	26	8	8	9	0	1	47	0	5	0	1	1	1	2	287.5	−0.2	17.109	274	223	2	16.0	1.6	2.1×10^{-11}	6.0
5341	96–250	18:51:01	2	2	2	189	10	13	14	14	14	0	1	1	38	15	5	0	1	1	1	2	287.5	−0.2	15.059	184	272	−56	2.5	1.6	7.4×10^{-11}	6.0
5347	96–250	18:57:16	2	2	2	106	15	4	2	0	5	12	0	0	4	0	5	0	1	1	1	2	287.5	−0.2	15.019	301	228	24	11.8	11.8	3.1×10^{-13}	5858.3
5369	96–250	19:28:24	8	3	3	133	20	22	17	6	10	9	0	1	40	0	5	0	1	1	1	2	287.5	−0.2	14.822	263	223	−6	15.0	1.6	3.7×10^{-12}	6.0
5381	96–250	20:17:56	8	3	5	105	49	49	28	10	15	8	0	1	47	0	5	0	1	1	1	2	287.5	−0.2	14.518	302	228	25	11.8	11.8	2.7×10^{-10}	5858.3
5388	96–250	20:53:19	8	3	3	99	21	25	12	8	9	8	0	1	46	0	5	0	1	1	1	2	287.5	−0.2	14.305	311	231	31	14.0	1.6	8.4×10^{-12}	6.0
5392	96–250	21:28:43	8	3	2	119	8	10	6	12	13	5	0	1	2	31	5	0	1	1	1	2	287.5	−0.2	14.095	283	224	9	5.9	1.6	2.3×10^{-12}	6.0
5412	96–250	23:21:57	8	2	4	99	27	29	26	10	9	2	1	1	45	3	5	0	1	1	1	2	287.5	−0.2	13.445	311	235	14	9.5	1.7	1.1×10^{-10}	7.6
5452	96–251	02:47:14	8	2	2	210	8	12	7	9	9	6	0	0	36	0	5	0	1	1	1	2	287.5	−0.2	12.376	155	310	−48	19.9	1.6	7.4×10^{-14}	6.0
5512	96–251	10:06:03	8	3	3	118	22	26	14	5	5	6	0	1	46	0	5	0	1	1	1	2	287.5	−0.2	10.854	284	224	10	40.9	1.6	2.4×10^{-13}	6.0
5534	96–251	14:35:00	8	2	2	174	14	20	0	15	14	12	0	0	22	0	5	0	1	1	1	2	287.5	−0.2	10.667	205	245	−48	2.5	1.6	2.9×10^{-10}	6.0
5535	96–251	16:16:06	100	2	2	109	14	20	15	11	8	7	0	1	36	0	5	0	1	1	1	2	287.5	−0.2	10.765	297	226	20	13.8	1.6	1.7×10^{-12}	6.0
5536	96–251	16:21:09	8	2	2	38	14	10	5	13	15	0	1	1	12	29	5	0	1	1	1	2	287.5	−0.2	10.772	37	317	40	2.3	1.9	1.3×10^{-10}	10.5
5537	96–251	17:24:51	8	2	2	134	9	22	4	9	2	10	0	0	10	0	5	0	1	1	1	2	287.5	−0.2	10.883	262	223	−7	12.7	1.9	1.3×10^{-12}	10.5
5538	96–251	17:39:01	8	3	4	127	24	27	26	7	9	9	0	1	46	0	5	0	1	1	1	2	287.5	−0.2	10.912	271	223	0	16.0	1.6	1.3×10^{-11}	6.0
5539	96–251	19:39:21	8	2	3	153	19	20	17	10	7	0	1	1	40	11	5	0	1	1	1	2	287.5	−0.2	11.224	235	228	−28	4.5	1.9	7.0×10^{-11}	10.5
5540	96–251	21:11:22	8	2	2	2	9	11	2	15	11	12	0	0	20	0	5	0	1	1	1	2	287.5	−0.2	11.535	87	333	1	6.4	3.1	2.1×10^{-12}	58.7
5543	96–252	07:27:08	8	2	2	252	9	11	0	14	5	13	0	0	47	2	5	0	1	1	1	2	287.5	−0.2	14.690	96	333	−5	11.8	9.5	3.9×10^{-13}	2690.1
5544	96–252	20:46:54	22	3	4	10	26	30	23	9	8	5	0	1	47	0	1	0	1	0	1	2	287.6	−0.2	19.873	76	332	10	13.8	1.6	4.2×10^{-11}	6.0
5550	96–255	01:49:04	22	3	4	222	29	49	29	12	15	5	0	1	19	0	1	0	1	0	1	2	287.8	−0.2	38.942	138	323	−38	2.0	1.9	5.1×10^{-08}	10.5
5552	96–258	12:00:04	22	3	4	25	29	49	28	13	15	9	0	1	47	0	1	0	1	0	1	2	288.2	−0.2	60.894	55	326	27	2.0	1.9	5.1×10^{-08}	10.5
5653	96–289	02:09:10	22	3	2	229	14	21	1	9	5	8	0	1	42	0	1	0	1	0	1	2	291.2	−0.2	108.151	128	331	−31	12.7	1.9	2.5×10^{-12}	10.5
6848	96–308	08:12:44	8	2	2	186	8	13	0	9	9	6	0	1	36	0	1	0	1	0	1	2	292.5	−0.3	36.621	188	269	−55	19.9	1.6	8.7×10^{-14}	6.0
7090	96–309	13:55:36	2	3	2	105	9	14	3	10	11	9	0	1	37	0	1	0	1	0	1	2	292.5	−0.3	26.089	302	232	25	14.0	1.6	4.2×10^{-13}	6.0

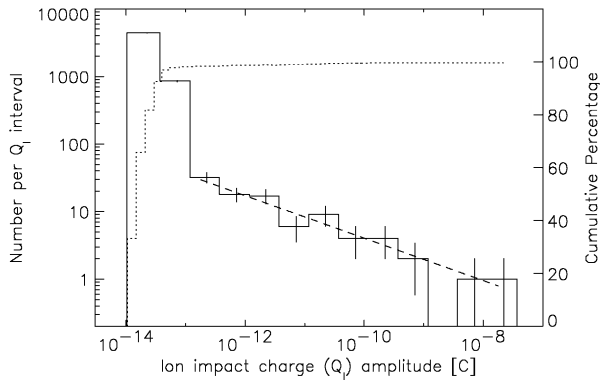| 7093	96–309	14:00:21	22	3	2	134	12	19	17	12	13	11	0	1	36	0	1	0	1	0	1	2	292.5	−0.3	26.059	262	227	−7	4.5	1.9	2.5×10^{-11}	10.5
7218	96–310	04:59:15	8	2	5	153	53	55	27	15	13	0	1	1	22	4	1	0	1	0	1	2	292.5	−0.3	20.156	235	231	−28	2.5	1.6	1.7×10^{-07}	6.0
7285	96–310	11:21:27	8	2	2	62	10	14	12	12	14	0	1	1	38	11	5	0	1	1	1	2	292.5	−0.3	17.509	3	285	53	3.8	1.6	2.1×10^{-11}	6.0
7385	96–310	23:44:37	8	3	2	94	10	13	3	11	12	8	0	1	4	31	5	0	1	1	1	2	292.5	−0.3	12.421	318	239	36	9.2	1.6	1.2×10^{-12}	6.0
7408	96–311	03:59:24	8	3	3	82	23	1	11	11	15	6	0	1	45	0	5	0	1	1	1	2	292.5	−0.3	10.919	335	251	46	2.3	1.9	9.3×10^{-11}	10.5
7436	96–311	06:06:49	8	2	3	152	22	22	20	12	11	0	1	1	47	31	5	0	1	1	1	2	292.5	−0.3	10.289	236	231	−27	2.0	1.9	2.9×10^{-09}	10.5
7438	96–311	06:49:17	8	2	2	174	9	12	6	12	13	0	1	1	40	14	5	0	1	1	1	2	292.5	−0.3	10.105	205	249	−49	5.9	1.6	3.2×10^{-12}	6.0
7439	96–311	09:03:45	8	3	2	3	15	20	17	11	9	10	0	1	37	31	5	0	1	1	1	2	292.5	−0.3	9.619	86	336	2	12.1	1.6	2.7×10^{-12}	6.0
7441	96–311	11:53:37	8	2	2	166	9	21	4	15	9	13	0	0	11	24	5	0	1	1	1	2	292.5	−0.3	9.262	217	240	−42	2.0	1.9	4.2×10^{-10}	10.5
7442	96–311	16:15:30	8	3	5	175	49	27	17	15	15	4	0	1	24	0	5	0	1	1	1	2	292.5	−0.3	9.365	204	250	−49	11.8	11.8	1.1×10^{-10}	5858.3
7444	96–311	16:36:44	8	3	2	226	10	12	2	10	10	8	0	1	37	0	5	0	1	1	1	2	292.5	−0.3	9.409	132	329	−34	16.0	1.6	2.4×10^{-13}	6.0
7445	96–311	17:46:30	259	3	3	85	20	21	4	8	7	10	0	1	40	0	5	0	1	1	1	2	292.5	−0.3	9.584	330	248	44	9.7	1.9	9.0×10^{-12}	10.5
7447	96–311	22:44:46	22	2	4	45	27	24	14	5	4	0	1	1	23	2	5	0	1	1	1	2	292.6	−0.3	10.825	27	313	45	29.8	1.9	1.2×10^{-12}	10.5
7448	96–312	01:13:24	8	2	2	254	9	12	0	15	11	12	0	0	3	31	5	0	1	1	1	2	292.6	−0.3	11.659	93	337	−3	6.4	3.1	2.5×10^{-12}	58.7
7449	96–312	01:13:24	8	2	3	24	20	13	21	10	15	0	1	1	47	28	5	0	1	1	1	2	292.6	−0.3	11.659	56	331	26	4.5	1.9	3.8×10^{-11}	10.5
7451	96–312	01:41:43	8	2	2	228	8	13	0	9	9	5	0	0	1	0	5	0	1	1	1	2	292.6	−0.3	11.829	129	330	−32	19.9	1.6	8.7×10^{-14}	6.0
7453	96–312	02:31:16	8	2	2	89	8	8	26	0	0	4	1	1	63	0	5	0	1	1	1	2	292.6	−0.3	12.134	325	243	40	11.8	11.8	2.0×10^{-13}	5858.3
7454	96–312	03:27:54	8	2	2	204	12	14	0	13	9	14	0	0	30	2	5	0	1	1	1	2	292.6	−0.3	12.491	163	305	−53	8.5	4.0	2.4×10^{-12}	138.9
7456	96–312	06:03:35	8	2	2	38	15	1	4	0	15	4	0	1	43	0	5	0	1	1	1	2	292.6	−0.3	13.514	37	336	38	11.8	11.8	2.0×10^{-13}	5858.3
7458	96–312	07:21:27	8	3	3	210	19	10	4	10	1	12	0	1	5	1	5	0	1	1	1	2	292.6	−0.3	14.042	155	331	−50	4.5	1.9	2.1×10^{-11}	10.5
7460	96–312	08:25:10	8	2	2	167	9	22	3	8	12	0	1	1	11	30	5	0	1	1	1	2	292.6	−0.3	14.479	215	256	−44	19.0	1.9	3.7×10^{-13}	10.5
7462	96–312	10:46:43	8	3	3	235	20	28	7	14	2	10	0	1	25	0	5	0	1	1	1	2	292.6	−0.3	15.463	120	350	−25	2.0	1.9	5.7×10^{-09}	10.5
7463	96–312	13:43:39	8	2	5	90	52	54	30	15	13	0	1	1	21	6	5	0	1	1	1	2	292.6	−0.3	16.704	323	259	38	2.5	1.6	1.3×10^{-07}	6.0
7464	96–312	19:09:13	22	3	5	43	49	52	30	15	14	5	0	1	47	0	1	0	1	0	1	2	292.6	−0.3	18.983	30	331	43	3.2	2.0	2.2×10^{-08}	12.5
7465	96–312	23:02:48	8	2	2	8	10	13	12	14	15	0	1	1	2	31	1	0	1	0	1	2	292.7	−0.3	20.593	79	336	8	2.1	1.6	1.5×10^{-10}	6.0
7469	96–314	00:45:44	22	2	4	62	25	31	11	15	4	4	1	1	23	0	1	0	1	0	1	2	292.8	−0.3	30.379	3	285	53	2.0	1.9	1.9×10^{-08}	10.5
7525	96–330	06:08:15	259	3	4	48	29	52	13	7	6	5	0	1	47	0	1	0	1	0	1	2	294.5	−0.3	88.246	23	315	48	12.7	1.9	2.3×10^{-10}	10.5
7789	96–350	20:31:24	22	2	2	148	15	5	9	0	0	8	0	0	0	0	1	0	1	0	1	2	296.1	−0.4	36.909	242	235	−22	11.8	11.8	3.6×10^{-13}	5858.3
7804	96–350	22:38:49	8	2	2	116	10	15	0	9	10	6	0	0	38	0	1	0	1	0	1	2	296.1	−0.4	36.243	287	234	13	18.3	1.6	2.3×10^{-13}	6.0
8109	96–352	23:57:20	8	2	6	169	59	57	27	6	12	4	1	1	31	0	1	0	1	0	1	2	296.2	−0.4	18.075	212	249	−44	19.0	1.9	2.2×10^{-09}	10.5
8145	96–353	06:33:40	22	3	2	71	11	21	1	14	4	14	0	1	10	0	1	0	1	0	1	2	296.2	−0.4	15.285	350	274	53	2.0	1.9	5.8×10^{-10}	10.5
8152	96–353	09:23:33	22	2	3	163	23	27	22	15	14	0	1	1	10	21	1	0	1	0	1	2	296.2	−0.4	14.103	221	244	−38	2.5	1.6	3.0×10^{-09}	6.0
8163	96–353	12:55:52	22	2	3	91	20	24	19	7	15	0	1	1	24	28	5	0	1	1	1	2	296.2	−0.4	12.676	322	247	39	6.4	1.6	5.1×10^{-11}	6.0
8184	96–353	19:39:19	22	3	2	59	11	14	7	15	15	8	0	1	47	3	5	0	1	1	1	2	296.2	−0.4	10.347	7	297	53	2.1	1.6	2.0×10^{-10}	6.0
8185	96–353	20:43:01	22	2	6	130	58	13	31	6	0	4	0	1	59	0	5	0	1	1	1	2	296.1	−0.4	10.062	267	232	−2	19.0	1.9	1.8×10^{-11}	10.5
8189	96–354	06:28:47	2	2	2	114	12	21	5	15	10	11	0	0	10	26	5	0	1	1	1	2	296.2	−0.4	9.369	290	234	15	2.0	1.9	6.9×10^{-10}	10.5
8193	96–354	06:51:05	2	2	2	110	10	12	13	10	10	2	1	1	6	31	5	0	1	1	1	2	296.2	−0.4	9.422	295	236	20	16.0	1.6	2.4×10^{-13}	6.0
8195	96–354	06:52:04	2	2	3	106	20	5	14	8	15	15	0	1	37	0	5	0	1	1	1	2	296.2	−0.4	9.425	301	237	24	9.7	1.9	9.6×10^{-13}	10.5
8197	96–354	06:54:00	2	3	2	139	10	13	14	11	12	8	0	1	2	31	5	0	1	1	1	2	296.2	−0.4	9.430	255	233	−12	9.2	1.6	1.2×10^{-12}	6.0
8198	96–354	06:54:53	2	2	2	140	9	12	8	12	13	4	1	1	34	31	5	0	1	1	1	2	296.2	−0.4	9.433	253	233	−13	5.9	1.6	3.2×10^{-12}	6.0
8200	96–354	06:55:57	2	2	2	109	14	20	18	11	8	7	0	1	39	31	5	0	1	1	1	2	296.2	−0.4	9.436	297	236	21	13.8	1.6	1.7×10^{-12}	6.0
8204	96–354	07:00:47	2	2	2	106	13	19	9	10	11	8	0	1	2	31	5	0	1	1	1	2	296.2	−0.4	9.450	301	237	24	8.6	1.6	3.9×10^{-12}	6.0
8205	96–354	07:08:33	2	2	5	150	49	11	17	15	0	5	0	1	58	0	5	0	1	1	1	2	296.2	−0.4	9.473	239	236	−25	11.8	11.8	1.1×10^{-11}	5858.3
8208	96–354	12:45:36	22	2	2	85	10	2	3	12	2	13	0	0	44	31	5	0	1	1	1	2	296.2	−0.4	10.933	330	253	45	4.5	1.9	1.8×10^{-12}	10.5
8209	96–354	13:06:50	22	3	2	11	11	25	4	14	15	13	0	1	63	10	5	0	1	1	1	2	296.2	−0.4	11.049	75	341	12	2.0	1.9	1.1×10^{-09}	10.5
8210	96–354	14:53:00	22	2	2	120	12	9	3	13	15	0	1	1	47	30	5	0	1	1	1	2	296.2	−0.4	11.659	281	233	9	2.3	1.9	7.9×10^{-11}	10.5
8211	96–354	14:53:00	22	3	3	160	20	22	18	6	10	11	0	1	39	0	5	0	1	1	1	2	296.2	−0.4	11.659	225	242	−35	15.0	1.6	3.7×10^{-12}	6.0
8212	96–354	15:56:42	22	2	2	131	11	49	18	9	11	0	1	1	28	20	5	0	1	1	1	2	296.2	−0.4	12.045	266	232	−3	12.7	1.9	1.1×10^{-11}	10.5
8213	96–354	18:04:05	22	2	2	247	13	22	8	14	11	0	1	1	49	30	5	0	1	1	1	2	296.2	−0.4	12.850	103	342	−10	2.0	1.9	9.5×10^{-10}	10.5
8214	96–354	23:50:55	8	2	4	13	26	7	26	8	0	9	0	1	35	19	5	0	1	1	1	2	296.2	−0.4	15.168	72	341	14	9.7	1.9	3.6×10^{-12}	10.5

Fig. 5. Amplitude distribution of the impact charge Q_I for the 5353 dust particles detected in 1996. The solid line indicates the number of impacts per charge interval, whereas the dotted line shows the cumulative distribution. Vertical bars indicate the $\sqrt{n}$ statistical fluctuation. A power law fit to the data for big particles with $Q_I > 10^{-13}$ C (AR2 to AR6) is shown as a dashed line (power law index -0.31).
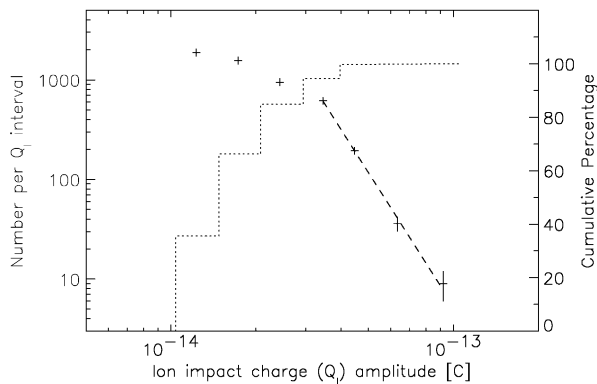

Fig. 7. Channeltron amplification factor $A = Q_C/Q_I$ as a function of impact charge Q_I for big particles (AR2–AR6) detected in 1996. The solid lines indicate the sensitivity threshold (lower left) and the saturation limit (upper right) of the channeltron. Squares indicate dust particle impacts, and the area of the squares is proportional to the number of events (the scaling of the squares is not the same as in earlier papers). The dotted horizontal line shows the mean value of the channeltron amplification $A = 1.8$ for ion impact charges 10^{-12} C $< Q_I < 10^{-10}$ C.

Fig. 6. Same as Fig. 5 but for the small particles in the lowest amplitude range (AR1) only. A power law fit to the data with 3×10^{-14} C $< Q_I < 10^{-13}$ C is shown as a dashed line (power law index -4.46).
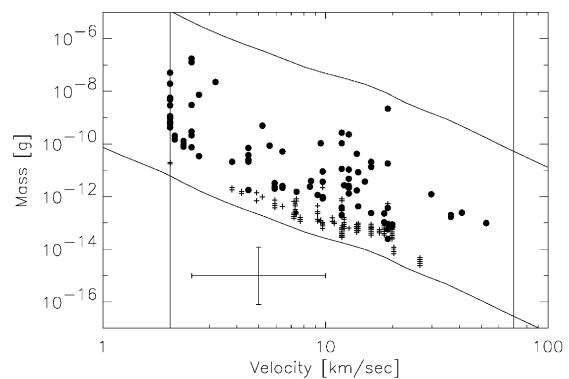
Fig. 8. Masses and impact speeds of all 5353 impacts recorded by DDS in 1996. The lower and upper solid lines indicate the threshold and saturation limits of the detector, respectively, and the vertical lines indicate the calibrated velocity range. A sample error bar is shown that indicates a factor of 2 error for the velocity and a factor of 10 for the mass determination. Note that the small particles (plus signs) are probably faster and smaller than implied by this diagram (see text for details).

threshold of DDS may not be sharp. The impact charge distribution for small particles with $Q_I > 3 \times 10^{-14}$ C follows a power law with index -4.5. This indicates that the size distribution of the small stream particles rises steeply towards smaller particles. It is much steeper than the distribution of the big particles shown in Fig. 5.

The ratio of the channeltron charge Q_C and the ion collector charge Q_I is a measure of the channeltron amplification A which is an important parameter for dust impact identification (Paper I). The in-flight channeltron amplification was determined in Papers II and IV for the initial 6 years of the Galileo mission to identify a possible degrading of the channeltron. For a channeltron high voltage of 1020 V (HV = 2) the amplification Q_C/Q_I obtained for 10^{-12} C $\leqslant Q_I \leqslant 10^{-10}$ C was $A \sim 1.6$ and ~ 1.4, respectively. Here we repeat the same analysis for the 1996 data set. Fig. 7 shows the charge ratio Q_C/Q_I as a function of Q_I for the same high voltage as in the previous papers. The

charge ratio Q_C/Q_I determined for 10^{-12} C $\leqslant Q_I \leqslant 10^{-10}$ C is $A \sim 1.8$. This is close to the earlier values and shows that there is no ageing of the channeltron detectable. Channeltron ageing is seen in the data after 1996 which will be the subject of a future publication.

Fig. 8 displays the calibrated masses and velocities of all 5353 dust grains detected in 1996. Impact velocities have been measured over almost the entire calibrated range from 2 to 70 km s^{-1}, and the masses vary over 8 orders of magnitude from 10^{-7} to 10^{-15} g. The mean errors are a factor of 2 for the velocity and a factor of 10 for the mass. Impact velocities below about 3 km s^{-1} should be treated with caution. Anomalous impacts onto the sensor grids or structures other than the target generally lead to

prolonged rise times of the charge signals. This in turn results in artificially low impact velocities and high dust particles masses.

The mass range populated by the particles is by two orders of magnitude smaller than that reported from the initial 6 years of the mission. The largest and smallest masses reported earlier, however, are at the edges of the calibrated velocity range of DDS and, hence, they are the most uncertain. Any clustering of the velocity values is due to discrete steps in the rise time measurement but this quantization is much smaller than the velocity uncertainty. Masses and velocities in the lowest amplitude range (AR1, particles indicated by plus signs) should be treated with caution. These are mostly Jovian stream particles for which we have clear indications that their masses and velocities are outside the calibrated range of DDS (Zook et al., 1996) (J. C. Liou, priv. comm.). The particles are probably much faster and smaller than implied in Fig. 8. On the other hand, the mass and velocity calibration is valid for the bigger particles (Krüger et al., 1999e, 2000). For many particles in the lowest two amplitude ranges (AR1 and AR2) the velocity had to be computed from the ion charge signal alone which leads to the striping in the lower mass range in Fig. 8 (most prominent above 10 km s^{-1}). In the higher amplitude ranges the velocity could normally be calculated from both the target and the ion charge signal which leads to a more continuous distribution in the mass-velocity plane.

Although no ageing of the channeltron could be found from Fig. 7 with the 1996 data set, other indications for ageing of DDS caused by the effects of the harsh radiation environment in the inner Jovian magnetosphere have been found: (1) The measured instrument current, which had a constant value of about 77.5 mA during the interplanetary cruise of Galileo, began to drop by 3% per year when the spacecraft was injected into the Jovian system in December 1995. This drop is most likely caused by radiation-induced ageing of a resistor and is inherent to the measurement process itself rather than being related to a real drop in the instrument current. (2) Changes in the test pulses generated by the instrument-built in test pulse generator. (3) A drift in the mean target and ion collector rise time signals ET and IT. Although it is best recognized in the data set for AR1, it may also affect the higher amplitude ranges. This drift does not affect the calibration of the 1996 data set but it may have to be taken into account in the mass and speed calibration of later data. The consequences of these ageing effects are under investigation and will be the subject of a future paper.

5. Discussion

By far the largest number of particles in the 1996 data set presented here are tiny dust grains originating from Io (Horányi et al., 1997; Grün et al., 1998; Graps et al., 2000;
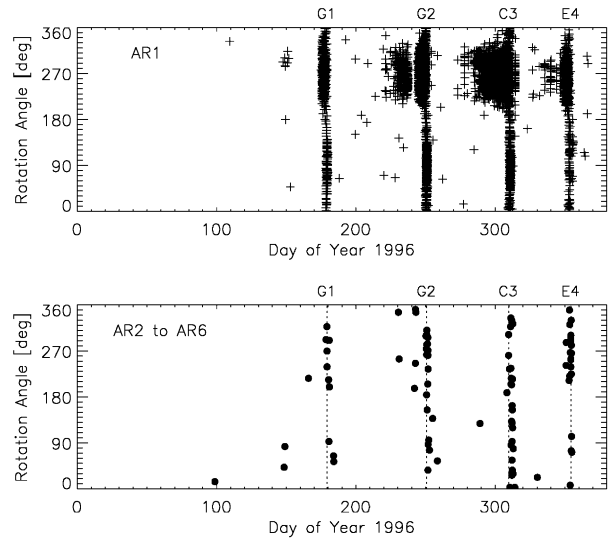

Fig. 9. Rotation angle vs. time for two different mass ranges, upper panel: small particles, AR1 (Io dust stream particles); lower panel: big particles, AR2 to AR6. See Section 2 for an explanation of the rotation angle. The encounters with the Galilean satellites are indicated by dashed vertical lines.

Heck, 1998). These grains almost exclusively populate amplitude range AR1 (see also Fig. 4, upper panel). They approach the sensor as collimated streams and their impact direction shows a characteristic behaviour that can only be explained by grains having a radius of about 10 nm and which strongly interact with the Jovian magnetosphere (Grün et al., 1998). The impact direction of these grains is shown in the upper panel of Fig. 9. On the inbound trajectory, when Galileo approaches Jupiter, the grains were mainly detected from rotation angles $270 \pm 70°$. This is best seen in the G2 and C3 orbits (1996, days 220–250 and 275–310) when we had continuous data coverage for the longest time period. One to two days before perijove passage the impact direction shifted by $180°$ and the particles approached from $90 \pm 70°$. Rotation angles of $90°$ and $270°$ are close to the ecliptic plane. The detection geometry is also seen in Fig. 1.

The tiny dust stream particles could be used for an analysis of the sensitive area of the Galileo dust sensor (Krüger et al., 1999c) which could not be done during ground calibration. A detailed analysis of the distribution of the measured rotation angles showed that three of the other instruments on board Galileo obscure the field of view of the dust sensor. This can be seen in the upper panel of Fig. 9 (see also Krüger et al., 1999c): there is a reduced number of particles with rotation angles ROT $= 270 \pm 20°$ in the G2 and C3 orbits when Galileo approaches Jupiter. This is best seen on days 200–225 and 270–285 in 1996. Fewer particles were detected in this time and rotation angle range with respect to the range ROT $= 310 \pm 20°$ and $230 \pm 20°$. This is caused by obscuration of the field of view.

Table 6
Times of the onset (class 3), 180° shift and cessation of the Jupiter dust streams[a]

Orbit	Onset class 3	180° shift	Cessation
G1	—	178.58 ± 0.05	—
G2	228.25 ± 3.9	250.20 ± 0.05	251.6 ± 0.1
C3	291.77 ± 1.7	310.20 ± 0.10	311.2 ± 0.1
E4	—	353.10 ± 0.10	354.4 ± 0.7

[a] When no entries are given, either no RTS data were obtained (onset in G1 and E4) or strong channeltron noise prevented the detection of dust impacts completely (cessation in G1).

Furthermore, the times of the onset of the dust impacts measured in classes 2 and 3 differ significantly which indicated that different sensitive areas apply to stream particles detected as classes 2 or 3 impacts, respectively. The times of the onset, 180°-shift and cessation of the dust streams are given in Table 6. Reliable onset times could be determined for class 3 and for orbits G2 and C3 only. For class 2 and for the other orbits no RTS data were obtained at the times of onset of the dust impacts. Note that Krüger et al. (1999c) used a larger data set for their analysis of the sensitive area of DDS which included data from 1997.

During the 180°-shift the detection rate of class 3 dropped significantly whereas no such drop was seen in the class 2 impact rate. This is consistent with a reduced field of view for class 3 w.r.t. class 2 and the reader is referred to Krüger et al. (1999c) for details. Especially, the shift for classes 2 and 3 occurred at the same time. Similarly, no time difference in the cessation of impacts in the two classes is noticable because at the cessation the dust streams sweep through the field of view rather quickly.

A periodogram (Scargle, 1982) of the dust impact rate measured in 1996 shows 5 and 10 h periodicities which are caused by the interaction of the dust grains with Jupiter's rotating magnetosphere (Fig. 10). Another strong peak occurs at Io's orbital frequency of 42 h. In addition, there are side lobes at Io's orbital frequency ± Jupiter's rotation frequency (10 h rotation period) or twice that frequency (5 h), respectively. If Io's orbital frequency is a carrier frequency, then the side frequencies show that Jupiter's rotation frequency amplitude-modulates Io's signal. Graps et al. (2000) have analysed a larger data set from 1996 and 1997 and used these findings—among other arguments—to conclude that Io is the source of the dust streams.

The lower panel of Fig. 9 shows the rotation angle for a second population of dust grains, namely bigger micrometer-sized grains. These grains are concentrated in the inner Jovian system forming a tenuous dust ring between the Galilean satellites. Modelling (Krivov et al., 2001) has shown that this ring is fed by particles escaping from impact-generated dust clouds around the Galilean moons (Krüger et al., 1999e, 2000). The impact directions and impact times imply that two groups of grains exist in the dust ring: particles on prograde and retrograde orbits about
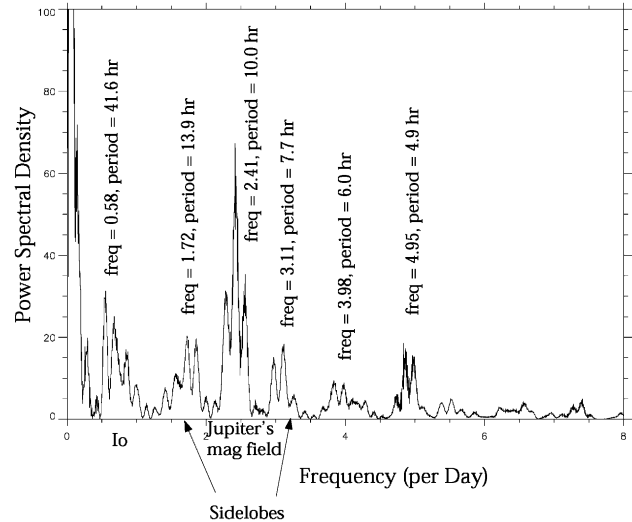

Fig. 10. A periodogram for the dust impact rate detected in 1996. See text for details.

Jupiter, respectively (Colwell et al., 1998; Thiessenhusen et al., 2000). Prograde particles are much more abundant than retrograde ones (Thiessenhusen et al., 2000). A fraction of the retrograde grains may be interplanetary or interstellar particles captured by the Jovian magnetosphere (Colwell et al., 1998).

References

Baguhl, M., Grün, E., Hamilton, D.P., Linkert, G., Riemann, R., Staubach, P., 1995. The flux of interstellar dust observed by Ulysses and Galileo. Space Sci. Rev. 72, 471–476.

Colwell, J.E., Horányi, M., Grün, E., 1998. Capture of interplanetary and interstellar dust by the Jovian magnetosphere. Science 280, 88–91.

D'Amario, L.A., Bright, L.E., Wolf, A.A., 1992. Galileo trajectory design. Space Sci. Rev. 60, 23–78.

Graps, A.L., Grün, E., Svedhem, H., Krüger, H., Horányi, M., Heck, A., Lammers, S., 2000. Io as a source of the Jovian dust streams. Nature 405, 48–50.

Grün, E., Baguhl, M., Divine, N., Fechtig, H., Hamilton, D.P., Hanner, M.S., Kissel, J., Lindblad, B.A., Linkert, D., Linkert, G., Mann, I., McDonnell, J.A.M., Morfill, G.E., Polanskey, C., Riemann, R., Schwehm, G., Siddique, N., Staubach, P., Zook, H.A., 1995a. Three years of Galileo dust data. Planet. Space Sci. 43, 953–969, Paper II.

Grün, E., Baguhl, M., Divine, N., Fechtig, H., Hamilton, D.P., Hanner, M.S., Kissel, J., Lindblad, B.A., Linkert, D., Linkert, G., Mann, I., McDonnell, J.A.M., Morfill, G.E., Polanskey, C., Riemann, R., Schwehm, G., Siddique, N., Staubach, P., Zook, H.A., 1995b. Two years of Ulysses dust data. Planet. Space Sci. 43, 971–999, Paper III.

Grün, E., Baguhl, M., Hamilton, D.P., Kissel, J., Linkert, D., Linkert, G., Riemann, R., 1995c. Reduction of Galileo and Ulysses dust data. Planet. Space Sci. 43, 941–951, Paper I.

Grün, E., Baguhl, M., Hamilton, D.P., Riemann, R., Zook, H.A., Dermott, S., Fechtig, H., Gustafson, B.A., Hanner, M.S., Horányi, M., Khurana, K.K., Kissel, J., Kivelson, M., Lindblad, B.A., Linkert, D., Linkert, G., Mann, I., McDonnell, J.A.M., Morfill, G.E., Polanskey, C., Schwehm, G., Srama, R., 1996a. Constraints from Galileo observations on the origin of jovian dust streams. Nature 381, 395–398.

Grün, E., Fechtig, H., Hanner, M.S., Kissel, J., Lindblad, B.A., Linkert, D., Maas, D., Morfill, G.E., Zook, H.A., 1992a. The Galileo dust detector. Space Sci. Rev. 60, 317–340.

Grün, E., Fechtig, H., Kissel, J., Linkert, D., Maas, D., McDonnell, J.A.M., Morfill, G.E., Schwehm, G., Zook, H.A., Giese, R.H., 1992b. The Ulysses dust experiment. Astron. Astrophys. Suppl. Ser. 92, 411–423.

Grün, E., Hamilton, D.P., Riemann, R., Dermott, S., Fechtig, H., Gustafson, B.A., Hanner, M.S., Heck, A., Horányi, M., Kissel, J., Kivelson, M., Krüger, H., Lindblad, B.A., Linkert, D., Linkert, G., Mann, I., McDonnell, J.A.M., Morfill, G.E., Polanskey, C., Schwehm, G., Srama, R., Zook, H.A., 1996b. Dust measurements during Galileo's approach to Jupiter and Io encounter. Science 274, 399–401.

Grün, E., Krüger, H., Graps, A., Hamilton, D.P., Heck, A., Linkert, G., Zook, H., Dermott, S., Fechtig, H., Gustafson, B., Hanner, M., Horányi, M., Kissel, J., Lindblad, B., Linkert, G., Mann, I., McDonnell, J.A.M., Morfill, G.E., Polanskey, C., Schwehm, G., Srama, R., 1998. Galileo observes electromagnetically coupled dust in the jovian magnetosphere. J. Geophys. Res. 103, 20,011–20,022.

Grün, E., Krüger, P., Dermott, S., Fechtig, H., Graps, A., Gustafson, B.A., Hamilton, D.P., Heck, A., Horányi, M., Kissel, J., Lindblad, B.A., Linkert, D., Linkert, G., Mann, I., McDonnell, J.A.M., Morfill, G.E., Polanskey, C., Schwehm, G., Srama, R., Zook, H.A., 1997. Dust measurements in the Jovian magnetosphere. Geophys. Res. Lett. 24, 2171–2174.

Grün, E., Zook, H.A., Baguhl, M., Balogh, A., Bame, S.J., Fechtig, H., Forsyth, R., Hanner, M.S., Horányi, M., Kissel, J., Lindblad, B.A., Linkert, D., Linkert, G., Mann, I., McDonnell, J.A.M., Morfill, G.E., Phillips, J.L., Polanskey, C., Schwehm, G., Siddique, N., Staubach, P., Svestka, J., Taylor, A., 1993. Discovery of Jovian dust streams and interstellar grains by the Ulysses spacecraft. Nature 362, 428–430.

Heck, A., 1998. Modellierung und Analyse der von der Raumsonde Galileo im Jupiter-system vorgefundenen Mikrometeoroiden-Populationen. Ph.D. Thesis, Ruprecht-Karls-Universität Heidelberg.

Horányi, M., Grün, E., Heck, A., 1997. Modeling the Galileo dust measurements at Jupiter. Geophys. Res. Lett. 24, 2175–2178.

Johnson, T.V., Yeates, C., Young, R., 1992. Galileo mission overview. Space Sci. Rev. 60, 3–21.

Krivov, A.V., Krüger, H., Grün, E., Thiessenhusen, K.–U., Hamilton, D.P., 2001. A tenuous dust ring of Jupiter formed by escaping ejecta from the Galilean satellites. J. Geophys. Res., submitted.

Krüger, H., Grün, E., Graps, A., Lammers, S., 1999a. In: Büchner, E.M.J., Axford, I., Vasyliunas, V. (Eds.), Proceedings of the VII. International Conference on Plasma Astrophysics and Space Physics, held in Lindau in May 1998, Vol. 264. Kluwer Academic Publishers, Dordrecht, pp. 247–256.

Krüger, H., Grün, E., Hamilton, D.P., Baguhl, M., Dermott, S., Fechtig, H., Gustafson, B.A., Hanner, M.S., Horányi, M., Kissel, J., Lindblad, B.A., Linkert, D., Linkert, G., Mann, I., McDonnell, J.A.M., Morfill, G.E., Polanskey, C., Riemann, R., Schwehm, G., Srama, R., Zook, H., 1999b. Three years of Galileo dust data: II. 1993 to 1995. Planet. Space Sci. 47, 85–106, Paper IV.

Krüger, H., Grün, E., Heck, A., Lammers, S., 1999c. Analysis of the sensor characteristics of the Galileo dust detector with collimated Jovian dust stream particles. Planet. Space Sci. 47, 1015–1028.

Krüger, H., Grün, E., Landgraf, M., Baguhl, M., Dermott, S., Fechtig, H., Gustafson, B.A., Hamilton, D.P., Hanner, M.S., Horányi, M., Kissel, J., Lindblad, B., Linkert, D., Linkert, G., Mann, I., McDonnell, J.A.M., Morfill, G.E., Polanskey, C., Schwehm, G., Srama, R., Zook, H., 1999d. Three years of Ulysses dust data: 1993 to 1995. Planet. Space Sci. 47, 363–383, Paper V.

Krüger, H., Grün, E., Landgraf, M., Dermott, S., Fechtig, H., Gustafson, B.A., Hamilton, D.P., Hanner, M.S., Horányi, M., Kissel, J., Lindblad, B., Linkert, D., Linkert, G., Mann, I., McDonnell, J.A.M., Morfill, G.E., Polanskey, C., Schwehm, G., Srama, R., Zook, H., 2001. Four years of Ulysses dust data: 1996 to 1999. Planet. Space Sci. Paper VII, submitted.

Krüger, H., Krivov, A.V., Grün, E., 2000. A dust cloud of Ganymede maintained by hypervelocity impacts of interplanetary micrometeoroids. Planet. Space Sci. 48, 1457–1471.

Krüger, H., Krivov, A.V., Hamilton, D.P., Grün, E., 1999e. Detection of an impact-generated dust cloud around Ganymede. Nature 399, 558–560.

Liou, J.–C., 1997. private communication.

Scargle, J.D., 1982. Studies in astronomical time series II.: statistical aspects of spectral analysis of unevenly spaced data. Astrophys. J. 263, 835–853.

Statman, J.I., Deutsch, L.J., 1997. In: Barbieri, C., Rahe, J.H., Johnson, T.V., Sohus, A.M. (Eds.), Proceedings of The Three Galileos: The Man, The Spacecraft, The Telescope. Kluwer Academic Publishers, Dordrecht, pp. 107–113.

Svestka, J., Auer, S., Baguhl, M., Grün, E., 1996. In: Gustafson, B.A., Hanner, M.S. (Eds.), Physics, Chemistry and Dynamics of Interplanetary Dust. ASP Conference Series, Vol. 104, pp. 31–34.

Thiessenhusen, K.–U., Krüger, H., Spahn, F., Grün, E., 2000. Dust grains around Jupiter—The observations of the Galileo Dust Detector. Icarus 144, 89–98.

Zook, H., Grün, E., Baguhl, M., Hamilton, D.P., Linkert, G., Linkert, D., Liou, J.–C., Forsyth, R., Phillips, J.L., 1996. Solar wind magnetic field bending of Jovian dust trajectories. Science 274, 1501–1503.